Simulation of dynamic expansion, contraction, and connectivity in a mountain stream network

Submitted for Publication in Advances in Water Resources

Adam S. Ward[1]
Noah M. Schmadel[1,2]
Steven M. Wondzell[3]

1. School of Public and Environmental Affairs, Indiana University, Bloomington, IN 47405, USA.
2. Now at U.S. Geological Survey, Reston, Virginia, USA
3. Pacific Northwest Research Station, Forest Service, United States Department of Agriculture.

Corresponding Author:
Adam S. Ward
School of Public and Environmental Affairs
Indiana University
430 MSB-II
Bloomington, IN 47405

Email: adamward@indiana.edu
Phone: 812-865-4820

Highlights:

- Implementation of a mechanistic, dynamic model of network expansion and contraction
- Importance of geologic setting and hydrologic forcing change through a water year
- Network expansion is insensitive to hydrologic forcing under wet conditions
- Geologic setting matters most under low and moderate discharge conditions
- Prediction of channel network dynamics may inform management of river corridors

Key Words:

- river corridor
- hyporheic
- solute tracer
- riparian
- network
- stream

Abstract:
Headwater stream networks expand and contract in response to changes in stream discharge. The changes in the extent of the stream network are also controlled by geologic or geomorphic setting – some reaches go dry even under relatively wet conditions, other reaches remain flowing under relatively dry conditions. While such patterns are well recognized, we currently lack tools to predict the extent of the stream network and the times and locations where the network is dry within large river networks. Here, we develop a perceptual model of the river corridor in a headwater mountainous catchment, translate this into a reduced-complexity mechanistic model, and implement the model to examine connectivity and network extent over an entire water year. Our model agreed reasonably well with our observations, showing that the extent and connectivity of the river network was most sensitive to hydrologic forcing under the lowest discharges (Q_{gauge} < 1 L s^{-1}), that at intermediate discharges (1 L s^{-1} < Q_{gauge} < 1 L s^{-1}) the extent of the network changed dramatically with changes in discharge, and that under wet conditions (Q_{gauge} > 1 L s^{-1}) the extent of the network was relatively insensitive to hydrologic forcing and was instead determined by the network topology. We do not expect that the specific thresholds observed in this study would be transferable to other catchments with different geology, topology, or hydrologic forcing. However, we expect that the general pattern should be robust: the dominant controls will shift from hydrologic forcing to geologic setting as discharge increases.. Further, our method is readily transferable as the model can be applied with minimal data requirements (a single stream gauge, a digital terrain model, and estimates of hydrogeologic properties) to estimate flow duration or connectivity along the river corridor in unstudied catchments. As the available information increases, the model could be better calibrated to match site-specific observations of network extent, locations of dry reaches, or solute break through curves as demonstrated in this study. Based on the low initial data requirements and ability to later tune the model to a specific site, we suggest example applications of this parsimonious model that may prove useful to both researchers and managers.

1. Introduction

The emerging river corridor perspective considers the surface stream, hyporheic zone, riparian zone, hillslope, and aquifer as a continuum, exchanging water, solutes, energy, and materials across a range of spatial and temporal scales (e.g., Harvey and Gooseff, 2015). Empirical studies have addressed dynamic connectivity along the river corridor at the network scale (e.g., Godsey and Kirchner, 2014, Gregory and Walling, 1968; Costigan et al., 2016), while others have documented the changes in ecosystem services and functions that result from connectivity in the riparian corridor (Boulton et al., 1998; Brunke and Gonser, 1997; Krause et al., 2011; Merill and Tonjes, 2014; US EPA, 2015). However, despite empirical advances, we lack an accurate framework to predict the temporal dynamics of hydrologic connectivity along the river corridor. Thus, an overarching objective of this study is to predict spatial and temporal patterns of hydrologic connectivity along the river corridor at the network scale. To achieve this objective, we synthesize our understanding of

how hydrologic forcing and geologic setting interact to control dynamic exchange processes in the river corridor, convert that understanding into a numerical model simulating the dominant processes in the river corridor, and implement the model at the network scale using readily available data. As a result, we derive and calibrate a mechanistic representation of dynamic hydrologic connectivity along the river corridor.

Hydrologic connectivity between the river corridor and its catchment, along the length of the river corridor, results from the geologic setting interacting with hydrologic forcing (Ward et al., 2016, 2014, 2012). The geologic setting is static at the time scales of interest here and includes the geologic constraint of the valley (e.g., D'Angelo et al., 1993; Stanford and Ward, 1993; Ward et al., 2016, 2012; Wondzell, 2006; Wright et al., 2005), channel and streambed morphology (Kasahara and Wondzell, 2003; see also review by Boano et al., 2014), and multi-scale heterogeneity in hydraulic conductivity of the valley floor sediment (e.g., Packman and Salehin, 2003; Ryan et al., 2004; Salehin et al., 2004; Sawyer and Cardenas, 2009; Vaux, 1968; Ward et al., 2011). Hydrologic forcing includes the lateral inflows to the valley bottom from either hillslope sources or from deeper groundwater and stream discharge – all of which vary with time and can thus lead to highly dynamic changes in connectivity. In mountain streams, the steep valley walls constrain the river corridor such that the entire valley bottom (stream, hyporheic zone, riparian zone) often can be collectively considered the river corridor.

Interactions between hydrologic forcing and geologic setting give rise to river corridor exchange across a wide range of spatial and temporal scales, driven by mechanisms including (after Kaser et al., 2009) turnover exchange (e.g., Elliott and Brooks, 1997a, 1997b; Packman et al., 2001), diffusion of turbulent momentum into the streambed (e.g., Malzone et al., 2016; Packman and Bencala, 2000), hydrostatically-driven exchange (e.g., Gooseff et al., 2006; Harvey and Bencala, 1993; Kasahara and Wondzell, 2003), and hydrodynamic pumping into the streambed and banks (e.g., Elliott and Brooks, 1997a, 1997b; Wörman et al., 2002).

Most studies examining exchange processes either assess one or just a small number of potential controls and most commonly within a short reach during baseflow conditions. Rarely are multiple controls studied over larger spatial and temporal scales. Consequently, the influence of individual factors are well understood at small spatial scales, but substantial challenges remain in aggregating the effects of multiple factors within a very long reach or an entire networks – the critical scales at which resources are managed and predictions are desired (Ward, 2015; Harvey and Gooseff, 2015).

The most widely applied strategy to translate process understanding in the river corridor to the reach or network scale uses reduced-complexity modeling. Bencala and Walters (1983) first developed their transient storage model, which was fit to solute breakthrough curves, to estimate advection, dispersion, and transient storage at the reach scale. This reduced-complexity modeling strategy eschewed the extensive parameterization required for distributed hydrologic models, but provided a mechanistic interpretation of processes that was absent from fully empirical models. While the transient storage model has been applied as a basis for understanding both short reaches and whole networks (Fernald et al.,

2001; Schmadel et al., 2014; Stewart et al., 2011), the model formulation is not able to simulate the dominant processes of mountain systems, where down-valley subsurface flow is important (Castro and Hornberger, 1991; Kennedy et al., 1984; Ward et al., 2016). Additionally, the transient storage model was never intended to represent dynamic network expansion and contraction, nor to accommodate spatially intermittent flows.

A second approach to upscaling river corridor exchange uses empirical relationships between catchment topology and river corridor processes based on field experiments (Covino et al., 2011; Mallard et al., 2014) or model experiments (Gomez-Velez et al., 2015; Gomez-Velez and Harvey, 2014; Kiel and Cardenas, 2014). These empirical approaches are readily implemented based on observable metrics (e.g., drainage area, stream discharge, sinuosity, streambed grain size). However, empirical approaches are site-specific in nature, with limited transferability across geologic settings and even to differing flow conditions. Studies based on model experiments assume the model processes simulated at one scale are the dominant processes across the continuum of nested scales of exchange in the river corridor.

Thirdly, distributed (or "top-down") hydrologic models build upon generalized knowledge, representing river corridor processes spanning spatial and temporal scales (Frei et al., 2009; Yu et al., 2016). A key strength of distributed models is their ability to represent heterogeneity, which may be important to determining intermittent connections between streams and their aquifers (Fleckenstein et al., 2007). However, distributed models require extensive parameterization and calibration, limiting their ability to be rapidly applied on the landscape.

While each of the existing approaches have been successful in advancing our understanding of specific mechanisms at a given spatial or temporal scale, these approaches all have limited ability to represent river corridor exchange in a way that is mechanistic, fully dynamic, and representative of the dominant processes within the network. Therefore, we suggest that a new predictive framework is needed – one that provides a mechanistic understanding of hydrologic connectivity along the river corridor, reflects the hydrologic dynamics that lead to time-variable connectivity, and would be readily transferable and scalable with modest data requirements. We propose a dominant process approach similar to Grayson and Blöschl (2000). This approach recognizes that reduced-complexity models will necessarily omit some processes in favor of representing those which are considered most important in a catchment (Smith et al., 2013). As such, we limit the over-parameterization of distributed models and avoid their problems with non-unique solutions (e.g., Beven, 2006, Bredehoeft and Konikow, 1993; Cardenas and Zlotnik, 2003; Oreskes et al., 1994; Poeter, 2007; Wondzell et al., 2009a). Here, we closely follow the approach of Smith et al. (2013) in identifying dominant processes based on our experience in the field, developing a perceptual model to explain our observations, and then implementing this perceptual model as a reduced-complexity model that simulates hydrologic processes at the scale of the river network.

Our primary objective is to predict spatial patterns and temporal dynamics of hydrologic connectivity along the river corridor at reach-to-network scales (i.e., 100s of meters and longer). A secondary objective is to develop an approach that is transferable, scalable, easily applied based on limited data requirements, and is flexible enough that increased data collection could be used to improve and refine the model at sites of interest. While Costigan et al. (2016) proposed a model of general meteorologic, geologic, and land cover trends that would be related to frequency of intermittency, their conceptual model does not address the dynamic transitions that occur between flow states, instead focusing on long-term trends. Specifically, we seek to answer the question: How do geologic setting and hydrologic forcing combine to result in dynamic connectivity along the river corridor? We hypothesize that geologic setting will be dominant during all baseflow conditions regardless of the actual discharge magnitude (i.e., during steady high, moderate, and low discharge conditions void of precipitation). Conversely, we hypothesize that network expansion and contraction will be dominated by hydrological inputs to the system during highly dynamic periods—such as storm event responses—that will cause rapid expansion and contraction of the network independently of the structure of the valley bottom. To test these hypotheses, we develop a reduced-complexity model in the spirit of the dominant-process approach. The model is calibrated at scales of 100s of meters to a well-documented solute tracer study and observed dry streambed locations, and validated based on stream stage observations at the field site. Using these results, we assess the dynamic interactions of hydrologic forcing and geologic setting, noting the places and times where each control is dominant.

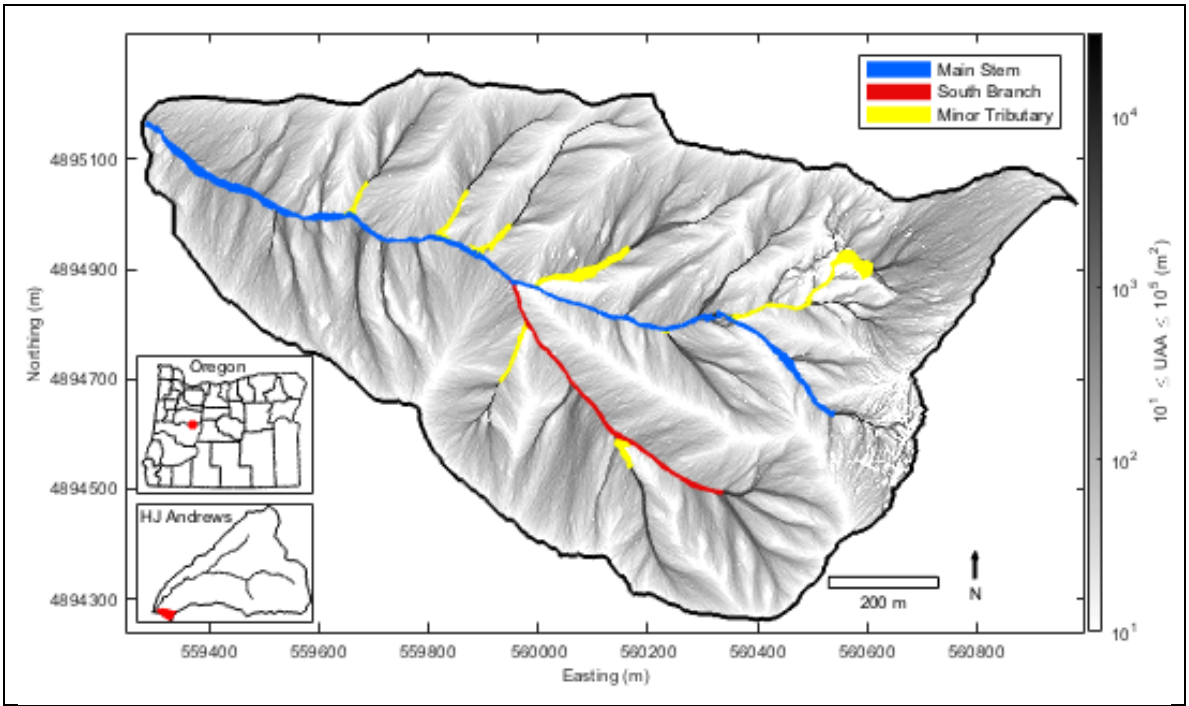

Figure 1. Watershed 1 (WS01) at the H.J. Andrews Experimental Forest in the western Cascades, Oregon, U.S.A. Upslope accumulated area (UAA) derived from a 1-

m LiDAR digital terrain model is shaded in greyscale. Valley segments draining more than 3 ha, defining the river corridor simulated in our model, are shown in color.

2. Background & Model Development

2.1 Site Description

The perceptual model presented here is based on extensive study of headwater mountain catchments in the western Cascades, Oregon, U.S.A., specifically the H.J. Andrews Experimental Forest. This site was selected based on the body of research documenting process dynamics in the river corridor of a mountain stream. Furthermore, this site fits the geological factors that Costigan et al. (2016) associate with increased intermittency including relatively large grain sizes, steep riffle morphology, impermeable lithology, and small drainage areas in a highly dissected catchment. This steep, geologically confined mountain stream network is also complimentary to recent efforts to model connectivity in low-gradient alluvial systems (Gomez-Velez et al., 2015; Gomez-Velez and Harvey, 2014; Kiel and Cardenas, 2014). Due to the high confinement of the valley bottom, the river corridor in this system is functionally equivalent to the valley bottom, which includes the stream, hyporheic zone, and riparian zone.

Within the H.J. Andrews Experimental Forest we selected the highly-studied Watershed 1 (WS01) as a study location because the dynamics of river corridor exchange have been studied in greater detail than other sites (Fig. 1). Briefly, this headwater catchment drains about 96 ha at the outlet stream gauge. Basin elevations range from 432 to 1010 m a.m.s.l. The catchment is highly dissected, with steep valley walls and hillslopes forming v-shaped valleys that are rapidly downcutting through Oligocene and lower Miocene aged volcanic bedrock. The longitudinal slope of the valley floor averages 11.9% (Voltz et al., 2013). In places the stream flows on exposed bedrock, but along most of its length, the valley bottom is covered in poorly-sorted colluvium, much of which was emplaced as landslide and debris-flow deposits. The depth of the colluvium ranges from 0 to at least 1.74 m, the deepest penetration achieved during installation of riparian monitoring wells (Wondzell, 2006). Precipitation data were collected at the nearby H.J. Andrews Primary Meteorological Station (about 0.5 km N of the gauge; elevation 430 m a.m.s.l.). Further physical description of the H.J. Andrews Experimental Forest and WS01 are available in a host of related publications (Dyrness, 1969; Swanson and James, 1975; Swanson and Jones, 2002; Voltz et al., 2013; Ward et al., 2016; Wondzell, 2006; Wondzell et al., 2009b).

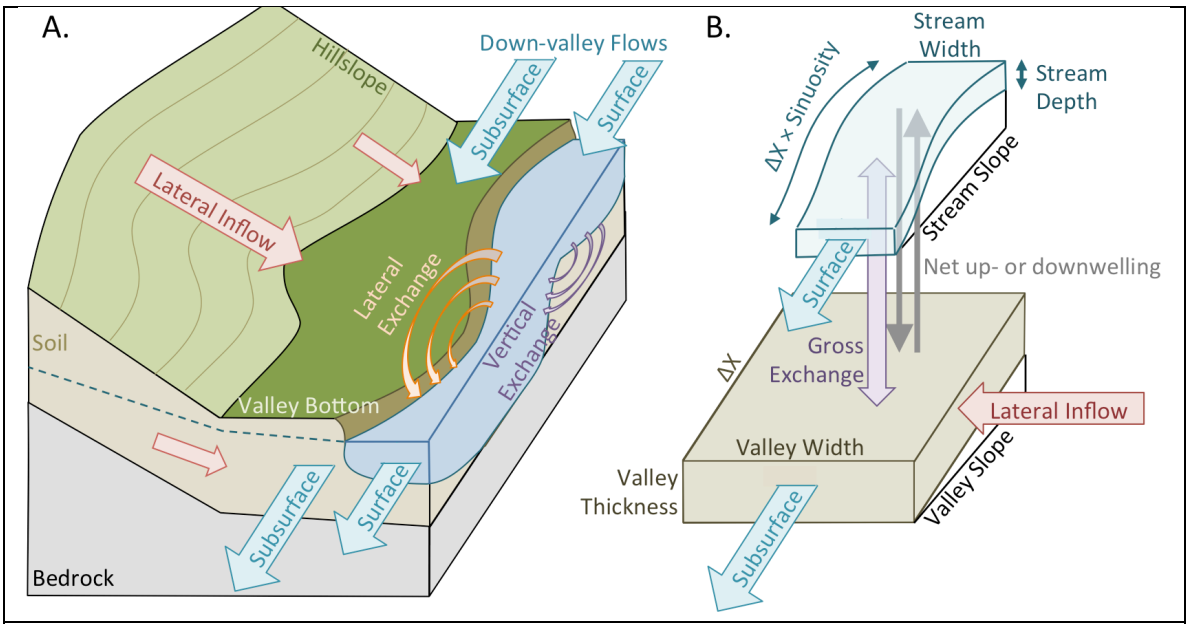

Figure 2. A) Perceptual model illustrating the dominant processes associated with river corridor exchange in headwater mountain streams. Key processes include down-valley flow in both the surface stream and subsurface porous media, smaller-scale exchanges in the vertical and lateral dimensions, confinement in the vertical (bedrock) and lateral (valley wall) dimensions, and lateral inflows proportional to upslope accumulated area from the hillslopes. B) Representation of dominant processes in the river corridor as a reduced-complexity model. The notation *x* refers to the along-valley coordinate (e.g., Δ*x* represents one spatial discretization of the model).

2.2 Perceptual Model of the River Corridor in Mountain Streams

We developed a perceptual model that explains dynamic expansion and contraction of the active channel network. A perceptual model is a qualitative representation of the dominant hydrologic processes operating at a given field site, integrating the processes that are known to be important based on field observations, numerical simulations, and a field-based understanding of the system (McGlynn et al., 2002, 1999; Sivapalan, 2003; Wagener et al., 2007). Thus, the model presented below is qualitative in nature, but synthesizes the observations of the site in a cohesive framework. This model is akin to a hypothesis explaining the interactions between geologic and hydrologic controls in the river corridor and is based on our current understanding developed over several decades of field studies at the site (Burt and McDonnell, 2015; Fig. 2A).

The perceptual model posits that the river corridor can be described as two parallel, interacting domains that transport water and solutes in the down-valley direction—via surface flows through the stream channel and via subsurface flows through the valley bottom (Ward et al., 2016). This builds directly from Bencala et al.'s (2011) notion that streams are dynamic expressions of the local groundwater system, and is well-aligned with the perceptual models of Godsey and Kirchner (2014) and Whiting and Godsey (2016). Subsurface transport in the down-valley

direction is known to be an important mechanism in higher-gradient stream networks (Castro and Hornberger, 1991; Jackman et al., 1984; Kennedy et al., 1984). Several studies have found relatively constant transport in the subsurface, attributing this primarily to an unchanging geologic setting (e.g., hydraulic conductivity field, major roughness elements, bedrock constraints, and valley width) and a down-valley hydraulic gradient set by topography (Voltz et al., 2013; Ward et al., 2016, 2014, 2012; Wondzell, 2006; Wondzell and Swanson, 1996). The primary mechanism of river corridor exchange in mountain streams is expected to be driven by hydrostatic pressure gradients (Wondzell and Gooseff, 2014; Schmadel et al., 2017). The down-valley subsurface discharge is functionally controlled by down-valley capacity, or the ability of the subsurface to transmit water through saturated porous media. In parallel, the surface stream flow represents only the excess of down-valley discharge that cannot be accommodated by the down-valley capacity. Thus, in-stream discharge and transport can be highly dynamic in response to the stream while transport in the saturated subsurface remains relatively constant. While subsurface down-valley discharge is relatively constant in time, it is spatially variable due to changes in the down-valley capacity of the subsurface, caused by changes in valley width, colluvium depth, slope, or heterogeneity in hydraulic conductivity.

The concept of spatially contiguous down-valley discharge is supported by the observed "long-term storage" of Ward et al. (2013a) in WS01. Their study found significant mass losses from stream solute tracer studies, concluding that the mass entered flowpaths that traveled down-valley but remained in the subsurface. Additionally, these flowpaths could not have been losses to a deeper groundwater aquifer because the river corridor is ultimately confined by intact bedrock.

Inputs of hillslope water to the valley bottom can affect the extent of long-term storage and these inputs vary in both space and time. Spatially, inputs from the hillslopes to the river corridor are assumed to vary in proportion with the contributing upslope accumulated area (UAA) after Jencso et al. (2009) and Corson-Rikert et al. (2016). Past studies in nearby catchments concluded that topography controls the transport of water from hillslopes to valley bottoms (e.g., McGuire et al., 2005). Discharge in the valley varies in time and impacts river corridor exchange during storm events (Ward et al., 2013a), seasonal baseflow recession (Ward et al., 2016, 2014, 2012), and diurnal fluctuations driven by evapotranspiration from riparian zones and perhaps the lower hillslopes (Schmadel et al., 2016; 2017; Voltz et al., 2013; Wondzell et al., 2010, 2007).

The upper reaches of the Main Stem and South Branch have surface flow during the winter and spring, but portions of them are frequently dry during the summer months (Fig. 1). We generally have not observed surface flow from convergent areas lateral to the main stem or south branch (i.e., those areas identified as "minor tributaries" in Fig. 1; Amatya et al., 2016). The colluvium accumulated within these areas is generally too deep and porous for the relatively small drainage areas to support surface flow. However, there are weakly developed channels, 10 to 30 cm wide, that suggest surface flow does occur during major storms in two specific conditions: (1) below bedrock outcrops where soils are quite shallow, forcing flow to the surface, and (2) high in the north-east corner of the

watershed where deep seated earthflows have created a drainage network around multiple small slumps where water may flow at the surface for much of the year. These areas are notable in that surface flow may occur with very small UAA, but they are always discontinuous to the channel network from which they are far removed (>50 m from the simulated channel network). Because of that, we do not consider them further in this study. Finally, both evapotranspiration from, and direct precipitation to, the valley bottom and stream are omitted given the small plan-view area of these landscape elements relative to the hillslopes.

2.3. Development of a Mathematical Model

The dominant processes in the perceptual model were translated into a numerical model (Fig. 2B). Subsequent sections describe the development of the surface and subsurface hydraulics, and the solute transport components of the model which are formulated for one-dimensional (1-D) segments of the valley bottom, with boundary conditions at the upstream end of each simulated segment.

2.3.1 Hydraulic Model

Open channel flow was simulated using the continuity equation and kinematic wave routing:

$$\frac{dA}{dt} + \frac{dQ_{str}}{dx} + \frac{Q_{up}}{dx} - \frac{Q_{down}}{dx} = 0 \qquad (1)$$

where t is time (s), x is the spatial coordinate along the valley bottom (m), A is the stream cross-sectional area (m^2), Q_{str} is the stream discharge ($m^3\ s^{-1}$), and Q_{up} and Q_{down} represent gross up- and downwelling flux ($m^3\ s^{-1}$), respectively. Net up- or downwelling flux (Q_{net}; $m^3\ s^{-1}$) is $Q_{net} = Q_{up} - Q_{down}$. We formulated the model using the gross exchanges to more accurately reflect the associated fluxes of solute (after Payn et al., 2008). Lateral inflows enter the model in the subsurface domain and represent either upwelling of valley bottom groundwater (unlikely in our case of bedrock constraint, but the term could be used for this flux in other settings) or lateral inputs of hillslope water, and influence the stream via the Q_{up} and Q_{down} terms. Thus, a term describing lateral inflows occurs only in the continuity equation applied to the subsurface domain (Equation 3). This formulation requires that lateral inflows to the simulated network do not consist of channelized overland flow. If that were the case, the simulated network should be expanded to include explicit simulation of any channelized flow at the surface. We relate discharge and channel geometry using Manning's equation:

$$Q_{str} = \frac{1}{n}\frac{A^{\frac{5}{3}}}{P^{\frac{2}{3}}}S_{Stream}{}^{\frac{1}{2}} \qquad (2)$$

where n is Manning's roughness coefficient (unitless), S_{stream} is the down-valley slope along the stream channel ($m\ m^{-1}$), the constant value of 1 in the numerator has associated units of $m^{1/3}\ s^{-1}$, and P is the wetted perimeter (m). We approximate the

stream geometry as a rectangular channel. Thus, $A = by$ and $P = b + 2y$, where b is the channel width (m) and y is the depth of flow in the surface channel (m).

In the subsurface, we solve the continuity equation for water as

$$\frac{dA_S}{dt} + \frac{dQ_{sub}}{dx} - \frac{Q_{up}}{dx} + \frac{Q_{down}}{dx} + \frac{Q_{lat}}{dx} = 0 \qquad (3)$$

where A_s is the cross-sectional area of the saturated portion of the subsurface (m^2), Q_{sub} is the down-valley subsurface discharge ($m^3\ s^{-1}$), and Q_{lat} represents lateral inflows from the hillslopes into the valley bottom ($m^3\ s^{-1}$), defined as the unit inflow per drainage area (q_{lat}) multiplied by the difference between UAA at the up- and downstream ends of the segment. All lateral inflows to the simulated network are assumed to occur in the subsurface; surface streams can initiate and combine at junctions if the down-valley discharge in a tributary exceeds down-valley capacity ($Q_{sub,cap}$; $m^3\ s^{-1}$). Darcy's law is used to calculate Q_{sub} as a function of valley width (b_{valley}; m), depth of subsurface flow (y_{sub}; m), hydraulic conductivity (K; $m\ s^{-1}$), porosity (θ, unitless), and valley slope (S_{valley}; $m\ m^{-1}$):

$$Q_{sub} = \frac{b_{valley} y_{sub} K}{\theta} S_{valley} \qquad (4)$$

We assume the slope of the valley bottom is a good approximation of the down-valley hydraulic gradient (Ward et al., 2016, 2013b; Wondzell, 2011). The maximum capacity of the subsurface to transport water in the down-valley direction (down-valley capacity; $Q_{sub,cap}$) occurs when $y_{sub} = T$, where T is the thickness of the valley bottom colluvium (m). Colluvium dimensions are related to geometry as $A_s = b_{valley} y_{sub}$. Total down-valley discharge (Q_{dv}; $m^3\ s^{-1}$) is the sum of surface and subsurface discharges:

$$Q_{dv} = Q_{str} + Q_{sub} \qquad (5)$$

2.3.2 Solute Transport Model

We solve for conservative solute mass in the surface using a volumetrically averaged mass balance for the stream:

$$\frac{d(VC)}{dt} = Q_{in} C_{in} - Q_{str} C + Q_{up} C_S - Q_{down} C \qquad (6)$$

where Q_{in} is the stream discharge from the upstream valley segment ($m^3\ s^{-1}$), C_{in} is the stream solute concentration from the upstream valley segment ($g\ m^{-3}$), C is the stream solute concentration ($g\ m^{-3}$), and C_S is solute concentration in the subsurface ($g\ m^{-3}$). The volume of water in the surface domain, (V; m^3), is calculated as:

$$V = Sinuosity * dx * b * y \qquad (7)$$

where *Sinuosity* is the sinuosity of the stream, calculated as the along-stream distance in each segment divided by the length of the segment ($m\ m^{-1}$).

For solute transport in the subsurface, we use a similar formulation:

$$\frac{d(V_S C_S)}{dt} = Q_{sub,in} C_{S,in} - Q_{sub} C_S - Q_{up} C_S + Q_{down} C + Q_{lat} C_{lat} \quad (8)$$

where $Q_{sub,in}$ is the subsurface discharge from the upstream valley segment ($m^3\ s^{-1}$), $C_{S,in}$ is the subsurface solute concentration from the upstream valley segment ($g\ m^{-3}$), C_{lat} is the concentration of lateral inflows from the hillslopes to the river corridor ($g\ m^{-3}$), and V_s is the volume of water in the subsurface domain (m^3), calculated as the volume of void space filled with water:

$$V_S = A_S \theta dx \quad (9)$$

For this formulation we assume that all pore space is connected for transport of water and solutes, and that the subsurface domain is well-mixed within each spatial discretization.

2.4 Model Implementation

2.4.1 Model Solution for Interior and Downstream Segments

The model equations presented above allow for spatially variable, dynamic activation of surface flow and continuity in space given the total down-valley flow and the amount that can be accommodated via the subsurface. We simulated transport through the river corridor at the network scale for water year 2016 (1-Oct-2015 through 30-Sept-2016). The model equations are implemented as a finite difference numerical solution along the river corridor, discretized using a 5-m segment length. Up- and downwelling fluxes (Q_{up} and Q_{down}) are calculated at each model segment on the basis of two logical operators, which operate to first assign all flow to the subsurface domain and then assign any flow exceeding $Q_{sub,cap}$ into the surface domain.

Channel water balance studies in mountain streams note that gross exchange of water between streams and their subsurface often exceeds net exchange (Covino et al., 2011; Payn et al., 2009; Ward et al., 2013b). To represent the gross up- and downward exchanges in the water balance, we define the parameter $Q_{subgrid}$ ($m^3\ s^{-1}$) to increase exchanges of water between surface and subsurface domains within each model segment.

For net up- or downwelling between the surface and subsurface domains, three possible behaviors exist. First, for cases when the flow entering a model segment is greater than the down-valley capacity (i.e., $Q_{sub,in} + Q_{lat} \geq Q_{sub,cap}$), net upwelling of the excess subsurface discharge is implemented:

$$Q_{down} = Q_{subgrid} \quad (10)$$

$$Q_{up} = (Q_{sub,in} + Q_{lat} - Q_{sub,cap}) + Q_{subgrid} \quad (11)$$

Second, for cases where the down-valley capacity is larger than the inflows to the

subsurface domain, net downwelling is required to ensure the full down-valley capacity is met before surface flow activates. Net downwelling is predicted for cases when $Q_{sub,in} + Q_{lat} < Q_{sub,cap}$. If the subsurface can accommodate the total down-valley discharge (i.e., $Q_{in} + Q_{sub,in} + Q_{lat} \leq Q_{sub,cap}$), all of the down-valley discharge is assigned to the subsurface, resulting in a dry streambed. Exchange discharges are, then:

$$Q_{down} = Q_{in} + Q_{subgrid} \quad (12)$$

$$Q_{up} = Q_{subgrid} \quad (13)$$

Finally, for cases of net downwelling (i.e., $Q_{sub,in} + Q_{lat} < Q_{sub,cap}$) where the subsurface cannot accommodate all of the down-valley discharge (i.e., $Q_{in} + Q_{sub,in} + Q_{lat} > Q_{sub,cap}$), stream discharge will occur. Vertical exchanges are, then:

$$Q_{down} = (Q_{sub,cap} - Q_{sub,in} - Q_{lat}) + Q_{subgrid} \quad (14)$$

$$Q_{up} = Q_{subgrid} \quad (15)$$

In this implementation, the down-valley capacity of the subsurface is always filled before the stream channel activates.

2.4.2 Boundary Conditions and Initial Conditions

For all model segments, initial conditions of $Q_{dv}(x,t=0)$, $C(x,t=0)$, and $C_s(x,t=0)$ are specified. The logical tests described above are used to partition $Q_{dv}(x,t=0)$ into Q_{str} and Q_{sub} fractions at $t=0$.

At the head of each channel (Fig. 1; Main Stem, South Branch, and all minor tributaries), specified boundary conditions of $Q_{dv}(x=x_n,t)$, $C(x=x_n,t)$, and $C_s(x=x_n,t)$ are required, where x_n is the upstream-most, or n^{th}, segment. We specify $C(x=x_n,t)= C_s(x=x_n,t)=0$ and $Q_{dv}(x=x_n,t)$ based on area-proportional discharge assigned from the gauge. This specification means that lateral inflows from the hillslope to the valley bottom are all synchronized in time to the stream gauge and does not allow for heterogeneity in hillslope responses to precipitation input. These simplifications are necessary to balance the desire for reduced-complexity with the representation of processes occurring in the landscape. For segments whose upstream end is the confluence of two tributaries, the discharge is defined as the sum of the outflows from the two upstream segments; the concentration is defined by conservative mixing of the two upstream tributaries.

With the time-variable boundary conditions established, the model equations are solved using a forward-in-time, backward-in-space solution scheme, which is computationally efficient and allows for an explicit solution of the model equations. We implement adaptive time stepping, allowing timesteps to grow or shrink by a factor of 4 depending on hydrologic and solute dynamics. Timesteps are limited in growth to constrain changes in discharge or concentration to less than 1% in a given timestep, with minimum and maximum timesteps of 1 and 3600 s, respectively.

2.5 Model Limitations

Implementation of the perceptual model as a reduced complexity model necessarily simplifies the processes in the river corridor to represent dynamics at reach-to-network scales. First, this simplification does not capture the smaller-scale flowpaths that are associated with individual channel-unit features smaller than 5 m in length. Instead, the 1-D representation of the valley bottom focuses on larger-scale, down-valley flow, and in our model, varies only in response to changes in valley width and longitudinal gradient. As a result, the spatial distributions of exchange fluxes or flowing status are not expected to have a high fidelity at representing individual features, but are expected to be representative at reach and longer scales (see Section 3.4 for reach-scale metrics). Therefore, we consider it inappropriate to expect performance to match small-scale patterns of intermittent flow that may develop because of individual features that are smaller than the spatial resolution of the model.

Second, the solute transport routine represents only advective processes along the stream, with numerical solutions introducing a small amount of numerical dispersion. The addition of longitudinal dispersion, transient storage, or sorption-desorption dynamics (e.g., after Bencala and Walters, 1983; Runkel, 1998) would likely improve the representation of solute transport. It is important to note, however, that we do simulate advective exchange between the surface and subsurface, but at spatial scales larger than 5 m. We also allow specification of surface-subsurface exchange occurring at scales smaller than 5 m, using the term $Q_{subgrid}$, but this term is treated as a constant across the entire network and thus cannot represent spatial variation in exchange processes driven by channel-unit features smaller than the resolution of the model. Collectively, surface-subsurface exchange is commonly considered to be an important component of transient storage. By contrast, fine-scale transient storage in the surface channel (i.e., in pools and eddies) is not simulated in our model because we expect surface-subsurface exchange to dominate at the scales we are simulating. Representing in-channel transient storage, longitudinal dispersion, and sorption-desorption would come at a computational cost. Further, several of these processes are likely sensitive to channel-unit scale features that cannot be extracted from typical airborne LiDAR data so including these processes in the model would likely require much more detailed data on stream topography.

Third, the assumption that all pore water is well mixed and equally connected is limiting. We acknowledge that the subsurface domain is likely not completely mixed over short timescales (e.g., Ward et al., 2012). Pores are recognized to range from fully connected to functionally disconnected from advective transport (e.g., dual-domain representations of porous media). This simplification also omits heterogeneity in the hydraulic conductivity, which has been shown to be an additional control on interactions between streams and their aquifers (e.g., Fleckenstein et al., 2007). In cases where the subsurface domain is not well-mixed, this assumption causes the exchanged mass to mix with a larger volume of water. The result is a slower equilibration between the stream and subsurface (i.e., concentrations in the subsurface rise and flush more slowly than would occur in a system that was not well-mixed). We do not consider these processes to be sufficiently important to be included in the perceptual model outlined above and are

thus not represented in the numerical model, but acknowledge these processes may be important at other sites.

Finally, the numerical model simplifies all hillslope hydrology as (1) instantaneously synchronized with discharge observed at the gauge and (2) discharge is proportionally distributed on the basis of upslope accumulated areas. Both are oversimplifications of catchment hydrology and hydraulics and are areas for potential future improvement.

3. Methods

The model derived above can be implemented using only a digital terrain model, a single stream gauge at the outlet of the catchment, and estimates of hydrogeologic properties. The highest uncertainty will likely come in the estimation of a representative hydraulic conductivity because this parameter is expected to span orders of magnitude. We suggest initial estimates based on any available data, grain size distributions, or modest field campaigns (e.g., falling-head tests in temporary piezometers or shallow wells) could be used to better constrain this model parameter. These modest data requirements are a key contribution of this relatively simple model. Again, we emphasize that reduced-complexity models are constructed to represent dominant mechanisms and interactions in a system of interest, acknowledging that this comes at the expense of representing complexity and heterogeneity of some processes in the system. In the following sections we detail how the model is parameterized using available data from our field site.

3.1 Model Parameters Specified for the Study Site

Implementing the model derived above requires analysis of stream, valley, and catchment topography to identify the drainage network, the valley floors, and the hillslope area contributing to each model segment. We used a modified version of the TopoToolbox (Schwanghart and Kuhn, 2010; Schwanghart and Scherler, 2014) to analyze the 1-m LiDAR digital terrain model available for WS01. We selected a spatial discretization of 5-m segments along the river corridor. Briefly, we applied the multidirectional flow routing algorithm (Seibert and McGlynn, 2007). Based on visual observations at the field site under high discharge conditions, we defined a threshold of 3 ha for channel initiation (i.e., all points where drainage area ≥ 3 ha are simulated as part of the river corridor). We selected the threshold of 3 ha because we seldom observe channelized flow in locations draining this small of an area. As a result, the upper extent of each simulated tributary should have no overland flow and the model equations are used to predict the flow initiation point along each headwater.

We measured the valley width at 30 locations, measuring from the stream centerline to the valley wall along a line perpendicular to the longitudinal axis of the valley (break-point visually identified in the field after Jencso et al., 2009). Our topographic analysis showed that the floodplain margin between hillslope and valley bottom was best approximated using an elevation 1.5 m above the streambed provided the best fit between widths extracted from the DEM and our field observations. Using that threshold, we discretized the stream network into 5-m segments and for each segment we extracted valley widths (left and right sides),

valley slope, stream channel slope, and stream channel sinuosity. We also calculated the lateral UAA along each side of the valley using TopoToolbox (Schwanghart and Kuhn, 2010; Schwanghart and Scherler, 2014).

Inflows to the valley bottom (Q_{lat}; $m^3\ s^{-1}$) were calculated using an area-weighted flow based on the WS01 gauge station. For each segment, the total lateral inflows were calculated as

$$Q_{lat} = \Delta UAA * Q_{gauge} / UAA_{gauge} \quad (16)$$

where ΔUAA is the change in UAA along the stream centerline in each model segment (ha), Q_{gauge} is the discharge at the WS01 stream gauge ($m^3\ s^{-1}$), and UAA_{gauge} is the UAA at the stream gauge (about 96 ha). The topographic analysis and area-weighted assignment of lateral inflows are identical to recent work in the catchment (Corson-Rikert et al., 2016). The gauge discharge data are used as published by the H.J. Andrews Experimental Forest. A summary of the specified or calibrated parameters are provided in Table 1.

Table 1: Sources and values for the model parameters.

Parameter	Value or range	Units	Methods and/or source
Channel width (b)	0.44 – 1.88	m	Regression with drainage area (Castro and Jackson, 2001)
Lateral inflow (q_{lat})	2.0×10^{-6} - 1.1×10^{-2}	$m^3\ s^{-1}$ per ha	Proportional to drainage area along stream centerline
Concentration of lateral inflow (C_{lat})	0	$g\ m^{-3}$	By definition for a tracer injected into the stream channel only
Manning's Roughness (n)	0.05	(unitless)	Visual inspection
Valley slope (S_{valley})	0.01 – 1.04	$m\ m^{-1}$	TopoToolbox analysis[1]
Channel slope (S_{stream})	0.01 – 2.42	$m\ m^{-1}$	TopoToolbox analysis[1]
Channel sinuosity ($Sinuosity$)	1.04 – 1.18	$m\ m^{-1}$	TopoToolbox analysis[1]
Valley width (b_{valley})	5.0 – 36.9	m	TopoToolbox analysis[1]
Drainage area (UAA)	3 – 95.5	ha	TopoToolbox analysis[1]
Porosity (θ)	0.3	(unitless)	Midpoint of previously reported range of values for the site (Dyrness, 1969; Kasahara and Wondzell, 2003; Ward et al., 2016; Wondzell et al., 2009a)
Sub-grid exchange ($Q_{subgrid}$)	4.18×10^{-5}	$m^3\ s^{-1}$	Calibrated. Parameter range 1×10^{-6} to 1×10^{-2} (Ward et al., 2013b)
Thickness of colluvium (T)	0.75	m	Calibrated. Parameter range 0 to 4 considered (Gooseff et al., 2006; Wondzell et al., 2009a)

Hydraulic conductivity (K)	5.62×10^{-6}	m s^{-1}	Calibrated. Parameter range 4.3×10^{-6} to 6.1×10^{-4} (Kasahara and Wondzell, 2003)
Limit to define surface discharge (Q_{lim})	2.21×10^{-4}	m^3 s^{-1}	Calibrated. Parameter range 0.18-0.32 (see section 4.1)

1 - TopoToolbox analysis refers to the analysis of the digital terrain model described in section 3.1 using tools developed by Schwanghart and Kuhn (2010) and Schwanghart and Scherler (2014).

3.2 Model Calibration

Recognizing the model limitations, we define two calibration targets that represent reach-scale behaviors to demonstrate reasonable representation of system processes: (1) reach-scale solute transport and (2) reach-scale fraction of dry streambed. These calibration targets will generate reach-averaged best-fit model parameters rather than spatially variable distributions, closely following the approach of other reduced-complexity models of headwater streams (e.g., Bencala and Walters, 1983).

First, we calibrated the model parameters T, K, and $Q_{subgrid}$ using a break-through curve from a solute tracer injection from 2-Aug-2010 (see Voltz et al., 2013; Ward et al., 2016 for details). We simulated the tracer injection and compared observed versus simulated concentrations of tracer at two locations: immediately downstream of the injection where complete mixing was assumed (166-m upstream of the WS01 gauge) and at the WS01 gauge station itself. We varied T from zero (observed at bedrock outcrops) to a maximum depth of 4 m. This greatly exceeds the maximum penetration depth of 1.74 m observed when installing wells, and thus allows for uncertainty between the refusal depth and impermeable bedrock. This difference may represent, for example, a zone of weathered bedrock below the colluvium but still bounded by impermeable, unweathered bedrock below. We varied K across the range of values observed by Kasahara and Wondzell (2003) in WS01 and a nearby headwater catchment, spanning 4.3×10^{-6} to 6.1×10^{-4} m s^{-1}. Finally, $Q_{subgrid}$ was varied from 1×10^{-6} to 1×10^{-2} m^3 s^{-1} based on observations at the field site. For comparison, Ward et al. (2013a) found average gross stream-to-subsurface exchanges of about 3.5×10^{-3} m^3 s^{-1} per 5 m of valley distance (range 0 – 1.6×10^{-2} m^3 s^{-1}, median 2.7×10^{-3} m^3 s^{-1}) during a storm event using reach-scale solute tracer studies. Thus, the range spans nearly the complete observation set (with a lower bound of 10^{-6} m^3 s^{-1} rather than zero). This first model calibration step was performed by uniformly sampling the distributions of K, T, and $Q_{subgrid}$ and varying the parameters jointly, increasing resolution around the best-fit parameters. More than 1,100 simulations were performed. Overall model fit was evaluated based on minimizing root mean square error (RMSE) between the observed tracer breakthrough curve and simulations. We selected minimizing RMSE because this is analogous to the residual sum of squared errors used to evaluate model fits in inverse modeling of stream solute tracers (e.g., Runkel, 1998; Ward et al., 2017).

Next, we calibrated the model by comparing the observed versus simulated total length of dry streambed in the reach of stream between the gauge and the confluence of the Main Stem and South Branch (Fig. 1). The model formulation

allows for computation of extremely small surface flows that would not be visually differentiated from a "damp streambed" or flow fully through the armored cobble layer on the bed in the field (e.g., values of $Q_{str} = 1\times10^{-4}$ m^3 s^{-1}). These simulated discharges are numerically non-zero, but functionally non-observable in the field. Thus, we require a threshold to differentiate observably flowing from dry segments in the model output (Q_{lim}). We select the target of total reach-scale dry streambed in acknowledgement that the reduced complexity model is not intended to represent small-scale features nor their spatial distributions that would be observed in the field, but instead to capture representative behavior for reaches 100s of meters and longer. This target is also comparable to reasonably available field data for a site with limited characterization, where available information may be based on visual inspection or personal knowledge that will typify applications lacking detailed site investigations (e.g., anecdotal "about 20% of the streambed is dry in late August"). On 25-May-2016, 21-June-2016, 04-July-2016, and 13-Aug-2016 we walked from the gauging station to the main confluence, recording the locations of dry streambed at sub-meter resolution. Using the specified parameters (Table 1) and those calibrated for the solute tracer (K, T, $Q_{subgrid}$), we assessed the accuracy of dry streambed predictions to select an appropriate value of the discharge threshold to define surface flow (Q_{lim}) to maximize accuracy of predicting the total dry length observed in the study reach.This calibration step tested more than 10,000 values for Q_{lim}, and selected the value that minimize the error in predicted dry streambed length along the observed reach.

3.3 Model Validation

To validate the model, we compared the flowing status predicted by the reduced complexity model with a similar dataset generated by combining a detailed survey with measured changes in stream stage. In the reach spanning 95 to 626 m upstream of the gauging station, we surveyed the elevation of the streambed and stream water surface at <1.0 m horizontal resolution and <0.01 vertical resolution during conditions with Q_{gauge} ranging from 5.8 to 6.7 L s^{-1}. Fifteen pressure transducers were installed along the surveyed reach, recording data every 15 minutes from 1-Oct-2015 to 2-Sept-2016. All loggers were installed in shallow wells to ensure they remained submerged all season even if water levels dropped below the streambed.

We constructed a spatially continuous water surface by calculating changes in the water surface elevation at each of the 15 sensors and then interpolating these changes to every model segment for each timestep. This exactly follows the procedures described by Schmadel et al. (2017). We then extracted the stream stage relative to the streambed for each 5-m segment within the surveyed reach and assigned a status of not flowing (for segments containing no surface flow), partially flowing (for segments with both surface flow and dry streambed), and fully flowing (for segments with active surface flow along the entire length of the segment). We assess reduced-complexity model performance by tabulating the frequency of correct predictions of flowing (times and locations where constructed profiles and model results both indicate fully flowing status) and correct predictions of not flowing (times and locations where constructed profiles indicate either partially or

not flowing status and the model predicts no flow). We elect to include "partially flowing" status from the profiles as equal to "not flowing" status in the reduced-complexity model because we expect the low discharges in a partially flowing segment would be below the calibrated Q_{lim} value.

3.4 Evaluation of Model Results: Spatial and Temporal Trends in Connectivity

Model results were used to evaluate nine metrics describing the hydrologic connectivity. For each river corridor segment, we tabulated: (1) the flowing status (i.e., surface flow or no surface flow), (2) subsurface discharge, and (3) surface discharge every 10 minutes throughout the 1-y simulation period. Based on this information and the network topology, we also tabulated (4) whether the surface flow was contiguous to the outlet (i.e., if there was an unbroken connection of surface flow between a segment and the outlet). Using these metrics, we next calculated (5) the total flowing length of the surface stream network, (6) the total contiguous length of the surface stream network, and (7) the drainage density (flowing stream network length per catchment area) for the flowing network. After completion of the entire 1-y simulation, we calculated (8) the probability of surface flow and (9) the probability of contiguous flow for each segment by dividing the number of timesteps with surface or contiguous flow by the total number of timesteps.

4. Results

4.1 Model Calibration & Validation

Overall, the calibrated model predicted the tracer breakthrough curve observed in August 2010 with an RMSE of 12.4 μS cm^{-1}. After calibration, we also assessed model predictions using r^2 (0.86 comparing time-series observations to calibrated model predictions), mean arrival time for the in-stream solute tracer timeseries (observed 75.6 hr, modeled 66.3 hr), coefficient of variation for the in-stream solute tracer timeseries (observed 0.72, modeled 0.70), and skewness for the in-stream solute tracer timeseries (observed 1.13, modeled 0.66). Based on the high r^2 and low errors for mean arrival time and coefficient of variation, we interpret that advection of the input tracer signal and its longitudinal spread are being accurately represented by the model. The disparity in skewness corresponds to the acknowledged limitations of the solute transport model, wherein only the advective transport processes are being considered. That the observed late-time low-concentration "tails" of the in-stream timeseries, which drive larger positive values of skewness, are not being well fit by the reduced-complexity model is expected given that longitudinal dispersion and in-channel transient storage are not simulated.

Next, we used observations of dry streambeds to estimate Q_{lim}. We did not observe any dry streambed during the May and June 2016 surveys. In July 2016 we observed a total of 3.5 m of dry streambed at 5 locations (range 0.5 to 1 m in dry length). In August 2016 we observed 106.1 m of dry streambed across 26 separate locations (range 0.4 to 26.9 m, mean 4.1 m, median 1.0 m). At the time of the August 2016 observations, the stream discharges in the model segments within the surveyed stream reach (0 m to 650 m from the stream gauge) ranged from 0.18 to

730 0.45 L s^{-1}. However, because our field observations recorded some of these
731 segments as dry, Q_{lim} must be greater than 0.18 L s^{-1} (i.e., discharges of less than Q_{lim}
732 were not observable as surface flow in the field). Furthermore, because discharge at
733 the gauge was measured between 0.32 and 0.45 L s^{-1} during the same period, this
734 also implies that Q_{lim} must be less than 0.32 L s^{-1}. We searched possible values for
735 Q_{lim} in this range at a resolution of 0.001 L s^{-1} (comparable to the resolution of the
736 gauge when the v-notch weir is installed during the summer low flow period). The
737 best agreement for total dry streambed length in the segment spanning 0 to 759 m
738 was found for Q_{lim} = 0.221 L s^{-1}, which results in a simulated 14.2% of the total
739 length in dry streambed conditions (compared to 13.9% observed in the field).
740 Using this value of Q_{lim}, the May and June 2016 simulation periods accurately predict
741 100% of the observed conditions in the field (Fig. S1). For July 2016 we observed
742 about 0.5% of the streambed to be dry (less than the length of one model segment)
743 and the reduced complexity model predicts all segments flowing fully (Fig. S1).
744 While the simulated length of dry channel was similar to that observed at the
745 reach scale, the agreement in the spatial location of dry segments was quite poor.
746 We expected considerable disagreement between the model and the observations
747 over short distances where small scale channel morphology – like wedges of
748 sediment accumulated above in-channel logs – would lead to local increases in
749 sediment thickness or create variable deposition environments leading to
750 substantial variability in saturated hydraulic conductivity. As expected, the model
751 did not simulate many of the short dry segments we observed, but it also simulated
752 a long dry section between 600 and 750 m above the stream gauge whereas we
753 observed large dry segments between 150 and 300 m. The lack of agreement
754 suggests that spatial patterning is being controlled by factors other than channel-
755 unit scale variations in morphology. Certainly, large logs transported in debris flows
756 can form large log jams with depositions several meters thick that extend more than
757 100-m upstream from the log jam. We used a constant thickness of 0.75 m resulting
758 from model calibration in a short tracer-injection reach near the bottom of the
759 watershed. Penetration depths of 41 wells located within that reach show that the
760 sediment thickness averages only 1 m and in early summer with Q_{gauge}=34 L s^{-1} the
761 saturated thickness averages 0.48 m. It is likely that sediment thickness at other
762 locations would be substantially deeper or shallower than the best-fit, reach-scale
763 value that was calibrated. Using a constant thickness would lead to the model
764 simulating dry channels in locations where the actual sediment was thinner than
765 0.75 m or wet channels in locations where the actual sediment is thicker than 0.75
766 m. Note that $Q_{sub,cap}$ is relatively constant from 750 m down to the mouth of the
767 watershed whereas UAA and Q both nearly double over this distance. Thus, small
768 overestimates of sediment thickness at the top of this reach would readily result in
769 the model simulating a dry channel where one may not be observed. Conversely,
770 limiting sediment thickness to only 0.75 m lower in the reach, where discharge is
771 much higher, would make it unlikely that the model would simulate a dry segment.
772 Finally, we compared the predictions of the stream status (flowing or dry) to
773 water surface profiles interpolated from 15 pressure transducers located in the
774 lower 650 m of the Main Stem channel. In total, we compared 99 model segments
775 spanning 32,443 timesteps that comprise approximately 3.2 million points (Fig. S2,

S3). Overall, the reduced-complexity model correctly predicted about 2.6 million flowing conditions (about 81.9% of all points; Fig. S2, S3) and 434,576 dry streambed conditions (about 13.5% of all points; Fig. S2, S3). The reduced complexity model incorrectly predicted 145,886 points (about 4.5% of all points; Fig. S2, S3). Based on more than 95% agreement between the model predictions and validation data, we are encouraged to interpret the model as a reasonable description of the dynamics in the system. Overall, model performance is generally strongest under higher discharge conditions. One key limitation of the model is the spatial resolution limits the simulation of segments that are partially flowing. While the network-scale metrics are reasonably predicted, the spatial organization is generally not well predicted by the model (Figs. S1, S2, S3) because of the assumed spatial homogeneity of model parameters.

The model could be further tuned by making T and K spatially variable. However, collecting spatially explicit data on sediment depth in the valley floor throughout the stream network would be a daunting task. But more importantly, adding substantial complexity to the model, just to improve the model fit, runs counter to the modeling philosophy that guides this effort. That is, to develop a highly transferable model that can be parameterized using readily available data to simulate dominant hydrological processes within a large stream network. We recognize that this simple model is far from perfect. Still, we argue that it represents the dominant hydrologic processes operating along the length of the stream network in this watershed.

4.2 Spatial Trends in Network-scale Hydrologic Connectivity

The study network is comprised of 2,825 m of stream channel (3 ha channel initiation threshold), equivalent to a channel density of 2.9 km km^{-2}. Valley topography, topology, slope, and sediment characteristics result in an average down-valley capacity ($Q_{sub,cap}$) of 4.6×10^{-2} L s^{-1} (range 1.2×10^{-3} to 3.7×10^{-1} L s^{-1}; median 3.7×10^{-2} L s^{-1}; Fig. 3A). Since network average values were used for T, K, and θ, this variation reflects the spatial variability in down-valley slopes and valley bottom widths in along the river corridor.

The probability of surface flow peaks at about 99.3% at the outlet of WS01 (Fig. 3B). The probability of surface flow decreases approximately linearly with distance to 93.0% at the confluence of the South Branch and Main Stem. The probability of surface flow decreases abruptly above the confluence in both branches due to the step decrease in tributary UAA (Fig. 3C). In both branches, probability of surface flow remains at or about 70% to a distance of about 1,100 m upstream from the outlet (about 330 m upstream of the confluence). Sharp changes in the probability of surface flow occur at locations where an increase in $Q_{sub,cap}$ accommodates the entire down-valley flow more frequently (for example, the Main Stem at 1150 m or the South Branch near 1,260 m; Fig. 3B). Overall, the probability of surface flow is lower in the upper Main Stem, upper South Branch, and the minor tributaries compared to the lower Main Stem below the confluence; this is due to the lower UAA in the upper basin (Fig. 3C).

The probability of surface flow throughout the network that is contiguous to the outlet is lower than the probability of surface flow in all cases, indicating periods

of time that dry locations along the valley break the contiguity of the network (Fig. 3D). The nearly perfectly horizontal portions of the probabilities across the plot (e.g., x = 850 to 1100 m along the South Branch; Fig. 3D) are caused by a downstream segment controlling the extent of contiguity up the branch. Although upstream segments are regularly flowing, they are prevented from becoming contiguous by a small location of sufficient down-valley capacity to prevent a contiguous surface connection from forming.

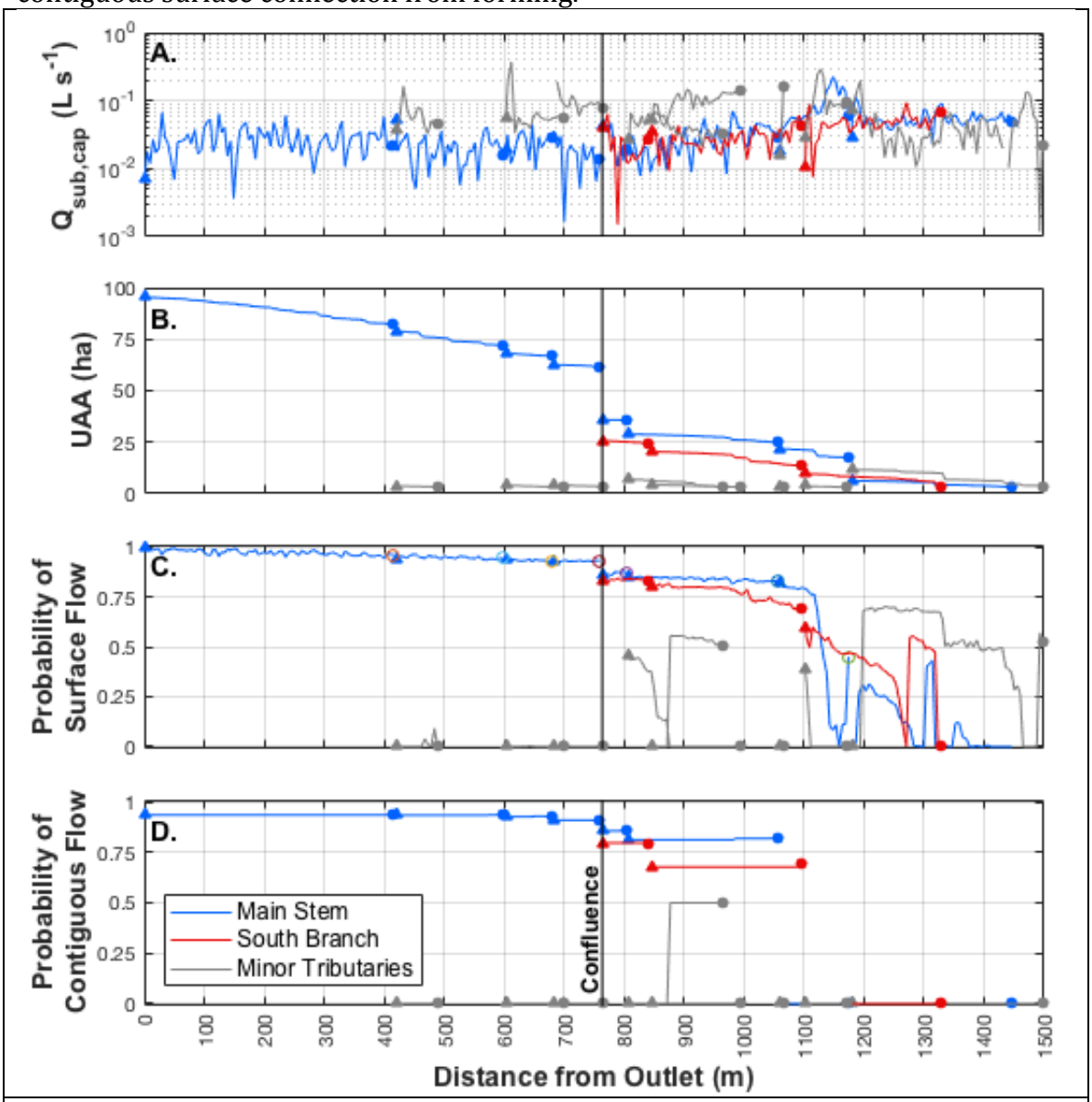

Figure 3. A) Down-valley capacity for subsurface flow ($Q_{sub,cap}$) as a function of distance along the river corridor from the outlet at the stream gauge. B) Probability of surface flow for each model segment. C) Upslope accumulated area (UAA) as a function of distance along the river corridor from the stream gauge. D) Probability of surface flow being contiguous to the stream gauge for each model segment. The vertical black line labeled "Confluence" denotes the confluence of the Main Stem and South Branch. For individual segments the upstream and downstream ends are

marked with circles and triangles, respectively.

4.3 Temporal Trends in Network-scale Hydrologic Connectivity

Throughout water year 2016 the length of the flowing network averaged about 1,661 m (range 0 to 2,350 m; median 1,810 m; Fig. 4B). Drainage density based on the flowing length averaged 1.73 km km^{-2} (range 0 to 2.45 km km^{-2}; median 1.89 km km^{-2}).

During the highest discharge conditions, the flowing channel network expands greatly, but small sections of dry streambed persist at some locations along the channel so only small increases in the contiguous length are simulated (callout 2 in Fig. 4A and 4B). Because of this, the fraction of contiguously flowing network decreases during the highest flow events (callout 2 in Fig. 4C). Under the lowest discharge conditions, the fraction of flowing length that is contiguous occasionally reaches a value of 1.0 (i.e., entirely contiguous) because only the downstream-most segments are predicted to have surface flow (e.g., callout 4 in Fig. 4).

The length of network contiguous to the outlet averaged 1,282 m (range 0 to 1,570 m, median 1,520 m; Fig. 4B). The contiguous network represents an average and maximum of 45% and 64%, respectively, of the river corridor length. The contiguous drainage density averaged 1.34 km km^{-2} (range 0 to 1.64 km km^{-2}; median 1.59 km km^{-2}). Throughout the water year, the contiguous network represented an average of 76% of the flowing network (i.e., 24% of flowing segments were not contiguous to the outlet; Fig. 4C). The fraction of the flowing network that was contiguous ranged from 0.8% to 100% across the year, with a median value of 77.5%.

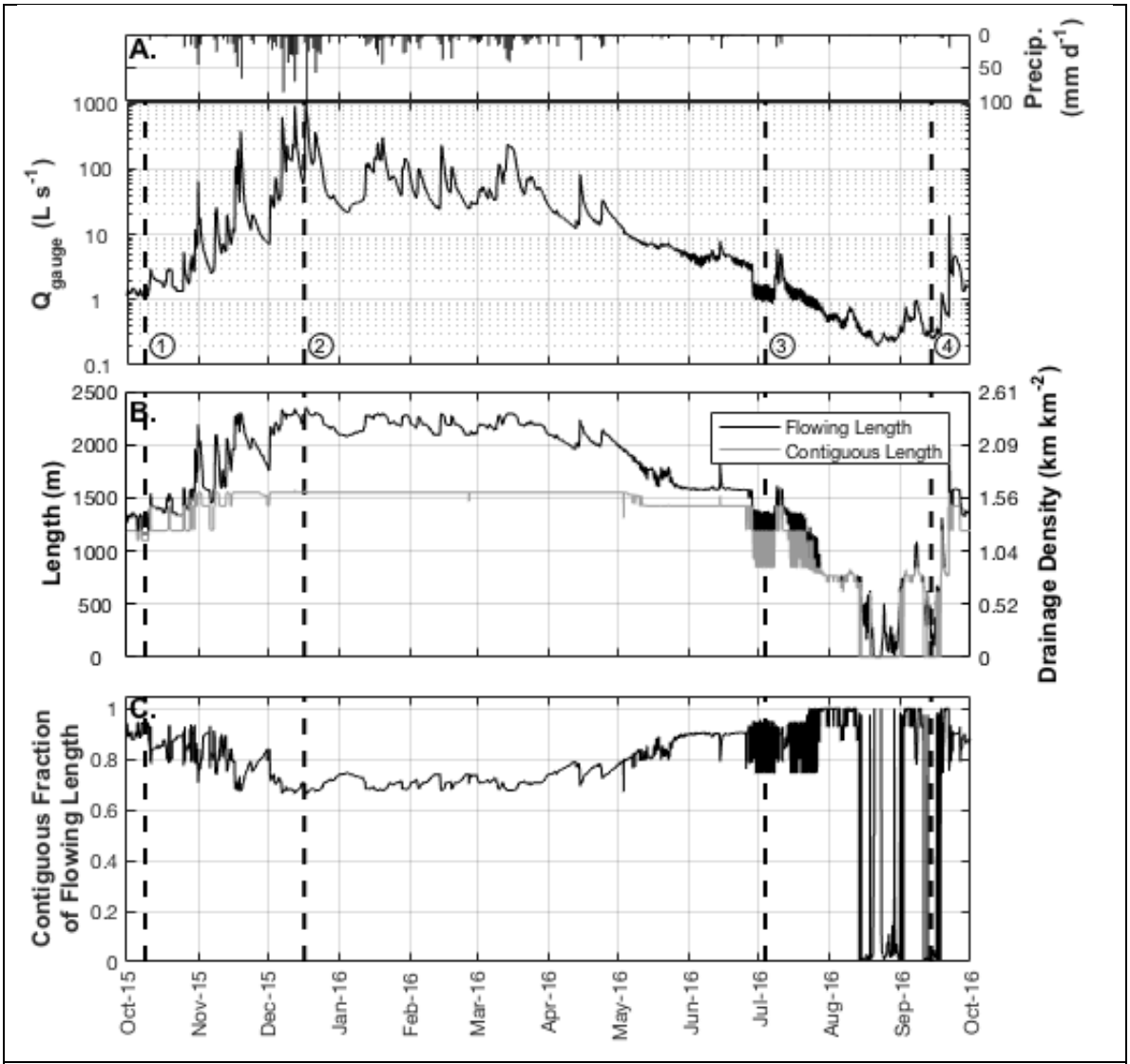

Figure 4. A) Water year 2016 discharge at the WS01 gauge and precipitation at the H.J. Andrews Primary Meteorological Station. B) Timeseries of total flowing length and total contiguous length along the river corridor. C) Timeseries of the fraction of flowing length that is contiguous to the gauge. Vertical dashed lines highlight the four timesteps shown in Figure 5 and are provided as a reference throughout Figs. 4-7. Finally, we note that a step-change decrease in discharge appears to occur on 28-June-2016 (from a peak discharge of 3.0 L s^{-1} on 27-June to 1.9 L s^{-1} on 28-June; panel A). This is a known discrepancy in the HJ Andrews discharge databases and results from installing v-notch weirs on the trapezoidal gauges to improve resolution of small changes in discharge. The V-notch weirs are typically installed in June and removed in October of each year (Henshaw and Creel, 2005). We use the stream discharge data as reported.

4.4 Spatial and Temporal Trends in Hydrologic Connectivity: Seasonal, Storm, and Diurnal Dynamics

Spatial patterns of surficial flow and contiguity are highly dynamic (Fig. 5; animation of water year 2016 in Supplemental Video). In many cases, a small number of short segments of dry streambed separate significant fractions of flowing streams from the outlet (Fig. 5), which is consistent with our field observations. Even in the highest discharge conditions, many of the minor tributaries do not generate surface flow (Fig. 5, second column). During the lowest discharge conditions, the subsurface transmits a majority of discharge in all but the downstream-most reaches (e.g., Fig. 5, fourth column). Under the highest discharge conditions the channel network expands significantly (e.g., Fig. 6B, callout 1). The newly activated surficial flows may persist for several days, or several months (e.g., Fig. 6B, callout 2, horizontal band of discharge about 1,320 m upstream of the outlet). Still, these locations are upstream of a persistently dry segment and never contribute to the contiguous length of the network, causing the gap between flowing and contiguous length (Fig. 4B). At locations of tributaries, there is a clear step change in discharge due to the step change in UAA at the confluence of the Main Stem and South Branch (visible as changes in color in the vertical direction; Fig. 6B, callout 3; Fig. 6C at 1,100 m upstream of outlet).

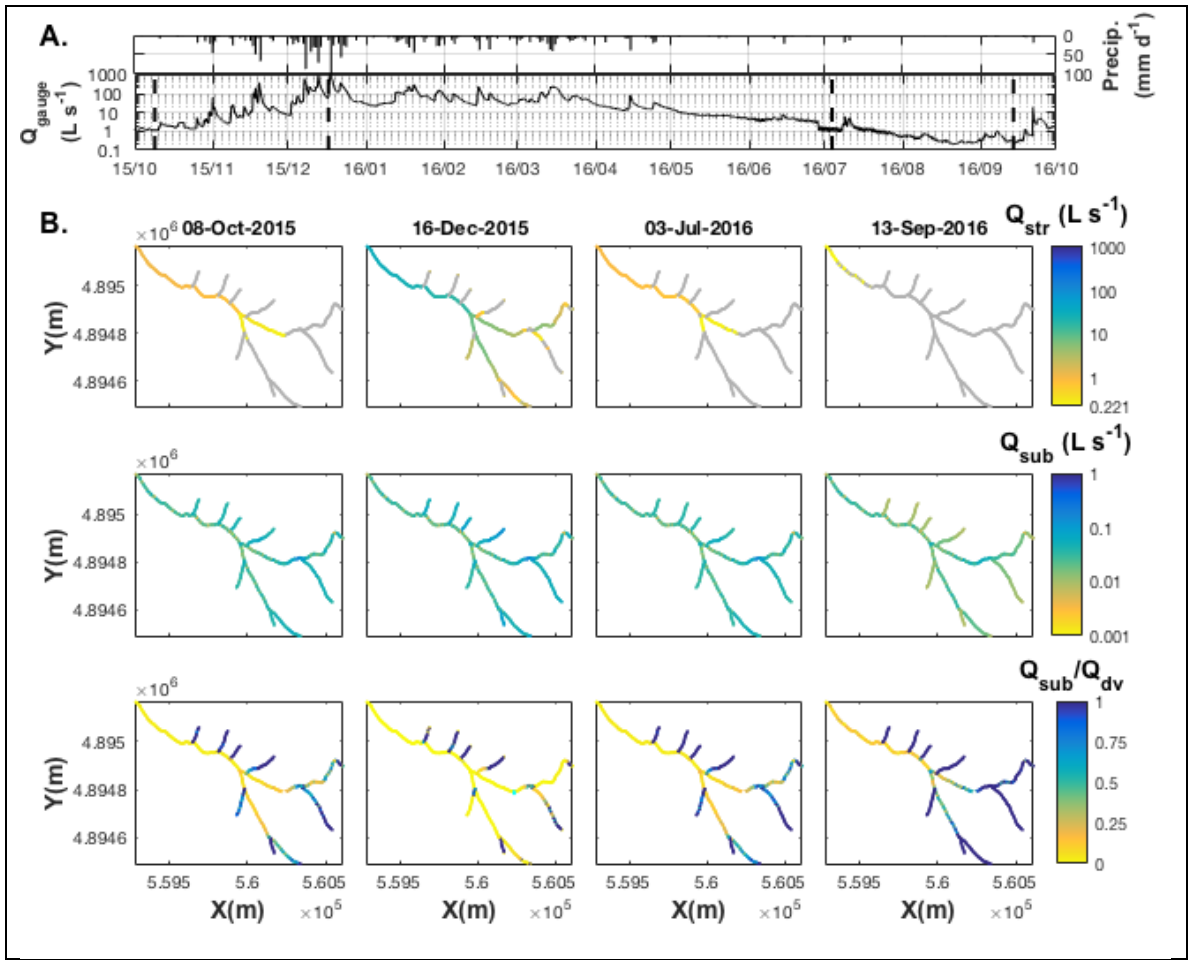

Figure 5. A) Water year 2016 discharge at the WS01 gauge and precipitation at the H.J. Andrews Primary Meteorological Station. B) Four snapshots in time of stream discharge (Q_{str}, top row), subsurface discharge (Q_{sub}, middle row), and fraction of total down-valley discharge in the subsurface (calculated as Q_{sub}/Q_{dv} or $Q_{sub}/(Q_{str}+Q_{sub})$). The dashed lines in the top panel correspond to the four columns of sub-plots (left-to-right). X and Y coordinates are listed in UTM Zone 10N.

For gauge discharges greater than about 1 L s^{-1}, the spatial extent of the network is relatively constant, extending to about 1,120 m along the Main Stem (Fig. 6B) and to 1,000 to 1,250 m along the South Branch (Fig. 6C). For gauge discharges less than about 1 L s^{-1}, the South Branch is mostly dry whereas the Main Stem, especially the lower 750 m, becomes temporally dynamic with large oscillations in the length of flowing channel. Significant contraction is observed during the lowest flow periods (Fig. 6B, callout 4). The first small storm of Fall 2016 (13.7 mm of rainfall from 2-Sept to 7-Sept-2016) causes rapid network expansion (visible as a nearly vertical line; Fig. 6B, callout 5).

The most frequent expansions and contractions of the channel network occur at the times when evapotranspiration-driven fluctuations in Q_{dv} (Voltz et al., 2013; Wondzell et al., 2010, 2007) cause Q_{dv} to fluctuate near $Q_{sub,cap}$, the threshold for surface flow (Fig. 7). In these cases, the flowing length and contiguous length can vary by hundreds of meters on a daily basis (Fig. 7B), which is confirmed by our field observations. In locations where the stream remains flowing we observe strong diurnal variations in discharge (visible as vertical bands in Fig. 7C).

A small storm delivered about 38.6 mm of rainfall between the 7th and 12th of July, 2016 (Fig. 7A). This rainfall caused a simulated expansion of more than 50% of the flowing (from about 900 to 1,650 m) and contiguous (from about 800 to 1,300 m) lengths of the channel network for a period of just 48 hours (Fig. 7B). Within four days, the discharge again reached a level where Q_{dv} and $Q_{sub,cap}$ were matched, reinitiating the daily oscillations in the flowing and contiguous channel lengths. Over the last half of July, baseflow recession continues, so that $Q_{sub,cap}$ exceeded Q_{dv} for longer and longer periods of each day, and over more and more of the length of the upper Main Stem, so that most channel segments were dry most of the time (Fig. 7C). This recession continues until all of the diurnal maximum discharge can be fully accommodated in the subsurface, at which point the channel remains dry until a storm in early September provides sufficient water to the catchment to reinitiate flow in the upper Main Stem (Fig. 6A and 6B).

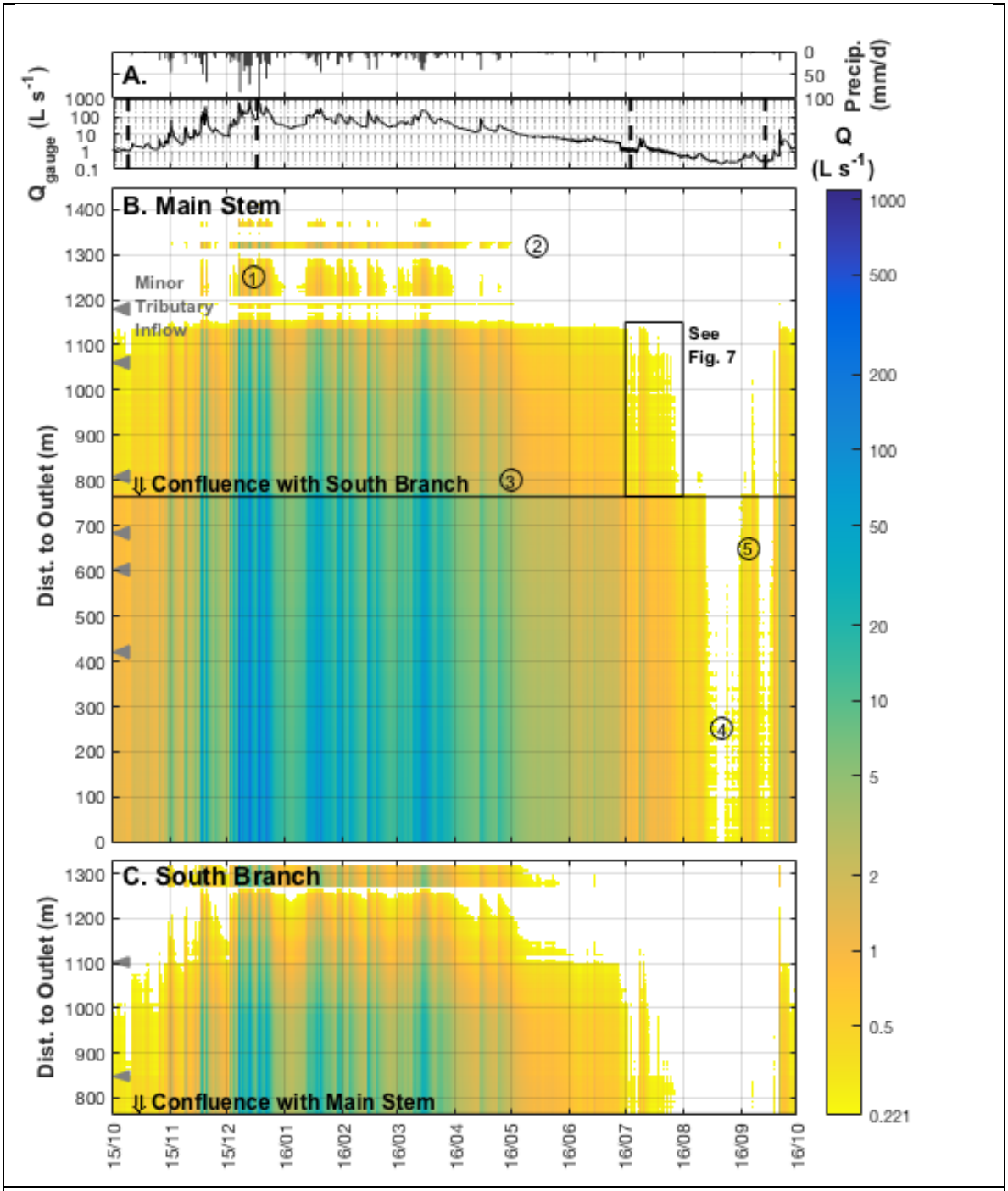

Figure 6. A) Discharge at the WS01 stream gauge and precipitation at the Primary Meteorological Station. Surface flow as a function of space and time in the Main Stem (panel B) and South Branch (panel C). Callouts in panel B highlight (1) surface flow under only the highest discharge conditions, (2) a relatively persistent location of disconnected surface flow high in the network, (3) a solid horizontal line marking a step-change in discharge at the confluence of the Main Stem and South Branch, (4) a nearly dry stream channel under seasonal low-flow conditions, and (5) rapid expansion in response to the first rain of Fall 2016. Unshaded (white) portions of

panels B and C represent places and times where $Q_{sub,cap}>Q_{dv}$, resulting in fully subsurface flow. The inset area is detailed in Figure 7. Black dashed lines in panel A correspond to those throughout Figs. 4-7.

904
905

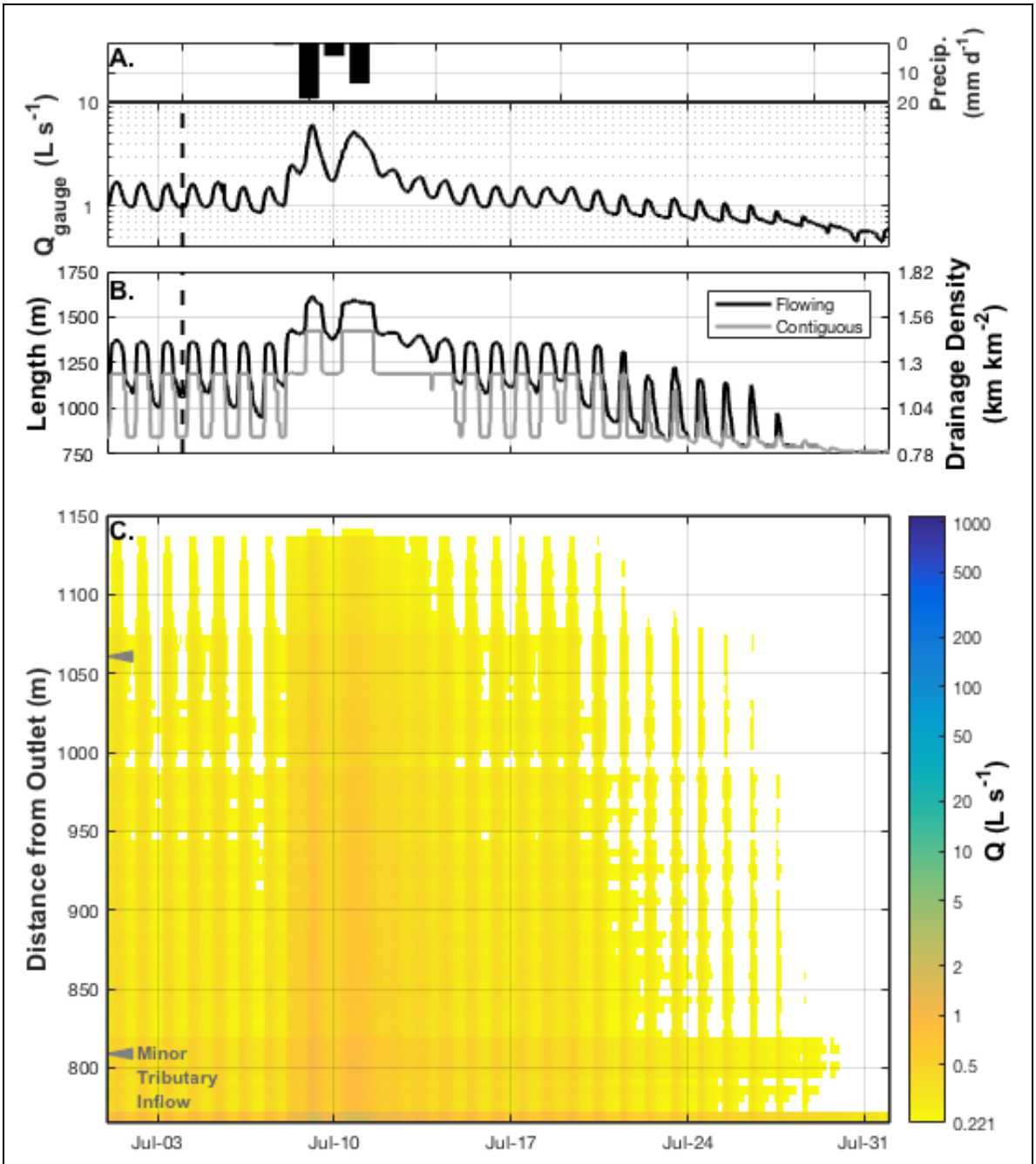

Figure 7. A) WS01 gauge discharge during baseflow recession of water year 2016 and precipitation at the Primary Meteorological Station. B) Dynamics of river corridor length with surface flow and contiguous surface flow to the gauge. C) Spatial and temporal dynamics of surface flow in response to diurnal discharge fluctuations driven by evapotranspiration (Voltz et al., 2013; Wondzell et al., 2010,

2007) and a small precipitation event. The black dashed line corresponds to the right-most vertical line in Figs. 4-6.

5. Discussion

5.1 Network Expansion, Contraction, and Connectivity Reflect Interactions of Hydrologic Forcing and Geologic Setting

Based on the simulated water year, we posit a systematic gradient from hydrologic to geologic control dominance as discharge decreases in the catchment. This finding agrees with empirical relationships developed by Godsey and Kirchner (2014), extending it to consideration through the full range of discharge conditions in the simulated water year.

The flowing length and contiguous length span relatively narrow ranges through the wet season (Oct. 2015 – Jul. 2016) despite Q_{gauge} varying across three orders of magnitude (Fig. 4A, 4B). Flowing length is about 1,800 m for Q_{gauge} = 8 L s^{-1}, increasingly to about 2,350 m for Q_{gauge} = 1,085 L s^{-1} ; for Q_{gauge} > 8 L s^{-1}, contiguous length is nearly constant at about 1,475 m (Fig. 8A). Under these high discharge conditions, the most important factors controlling the extent of the stream network are related to overall wet conditions. The hillslopes are contributing water to the valley bottom throughout the catchment and the valley bottom is saturated (i.e., $y_{sub} = T$). Thus, new rainstorms simply increase delivery of water from the hillslopes to the river corridor which is then transferred to the stream channel because Q_{dv} already exceeds $Q_{sub,cap}$. Further, spatial variation in $Q_{sub,cap}$, caused by variation in valley floor width (b_{sub}) and longitudinal gradient (S_{valley}), is small relative to Q_{dv}. Thus, the network extent is relatively insensitive to hydrologic dynamics.

The network responds dynamically to storm events under moderate flow conditions ($1 < Q_{gauge} < 8$ L s^{-1}; Fig. 8A). Under these moderate conditions, Q_{dv} is near $Q_{sub,cap}$. Thus, precipitation delivers water to the catchment, increases Q_{dv} and temporarily extends the upper end of the flowing network. As a result, both the flowing and contiguous lengths are highly variable in this range of discharges. The variability in flowing length is primarily associated with the transient activation of locations draining less than 10 ha (Fig. 8B). Thus, 10 ha UAA is an apparent threshold for the initiation of surface flow. The probability of surface flow or contiguous flow increases rapidly as UAA increases from zero to this 10 ha threshold. Locations draining more than 10 ha have surface flow more than 70% of the year.

The rapid expansion of the flowing and contiguous network in response to storm events under moderate flow conditions demonstrates the importance of interacting geologic setting and hydrologic forcing under these conditions. Under any given hydrologic condition, the upper extent of the drainage network reflects locations where enough drainage area is accumulated for Q_{dv} to exceed $Q_{sub,cap}$. However, UAA is not accumulated uniformly with distance along the stream network. Rather, it shows sharp jumps at tributary junctions, and especially at the confluence between the South Branch and Main Stem. These tributary junctions, then, create sharp discontinuities in the relation between discharge and both

flowing and contiguous channel lengths (Fig. 8A). Thus the watershed topology – the arrangement of hillslope contributing areas and tributary locations – emerges as a dominant control, defining the locations and relative fluxes of water into the river corridor (as also found in mountain stream networks by Jencso et al., 2009).

The changes in $Q_{sub,cap}$ due to valley morphology grow in importance as Q_{dv} and $Q_{sub,cap}$ become closer in magnitude (i.e., $Q_{dv} \approx Q_{sub,cap}$). This is readily seen in the model simulations at very low discharge conditions ($Q_{gauge} < 1$ L s^{-1}; Fig. 8A). During these low discharge conditions the river corridor becomes highly sensitive to hydrologic forcing. As such, even the relatively small diurnal fluctuations in Q_{dv} (Fig. 7) cause extensive network expansion and contraction. At locations where the valley widens, $Q_{sub,cap}$ increases and the stream network dries; where the valley narrows, $Q_{sub,cap}$ decreases and flow is reinitiated. Thus, geologic factors determining valley width and slope controls the network expansion and contraction in our model. In cases where heterogeneous K is considered, the variation of K across orders of magnitude may be the dominant control. Under these conditions, the storage of water in the catchment and its release as baseflow become important controls on when and where surface flow will emerge. Importantly, there is likely a condition of extremely low discharges in which this sensitivity would disappear because minor changes in down-valley discharge could be fully transported in the subsurface without activating the surface network (i.e., when $Q_{dv} << Q_{sub,cap}$).

While the thresholds described above are specific to our study site, the general transition to increasing importance of geologic controls under low discharges adds a dynamic context to the perceptual model we posed in Section 2. We expect that the perceptual model and the systematic transitions described above will be consistent across mountain stream networks. While the specific discharge and area thresholds will vary depending upon, for example, flow generation processes from the hillslopes, the general behavior is consistent with the relationships already described in the literature (Godsey and Kirchner, 2014). Still, this study contributes a dynamic perspective on the activation of the flowing stream network, including variation in space. The geologic controls we use (slope, valley width and depth, hydraulic conductivity) to estimate down-valley capacity are not included in Costigan et al.'s (2016) framework, which is framed to more broadly identify the types of landscapes in which intermittent flow may occur. Instead, our work highlights spatial variation in specific process controls and their manifestation as patterns of stream intermittency.

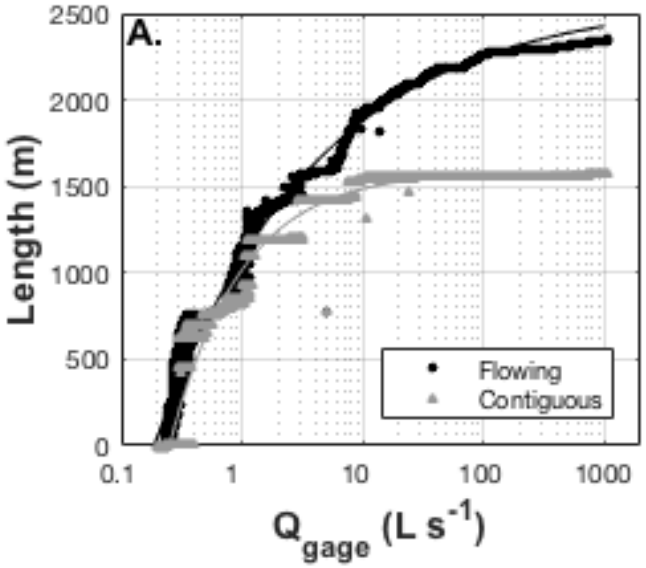

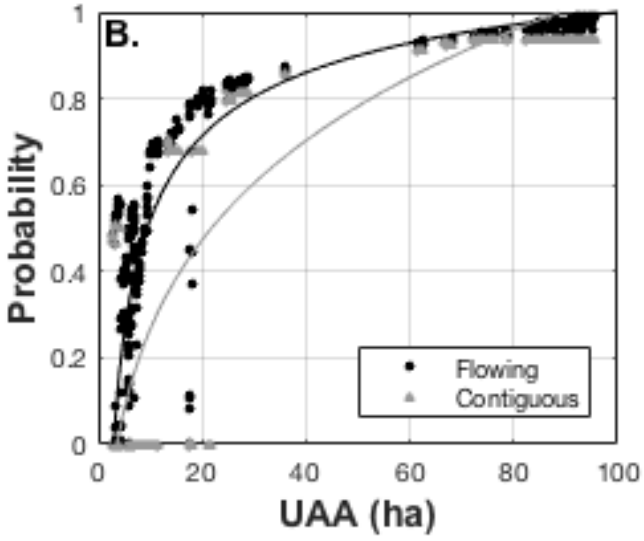

Figure 8. A) Flowing and contiguous lengths as a function of discharge at the WS01 gauge, showing a threshold in contiguous length at about 8 L s^{-1}. B) The probability of surface flow (black) and contiguous surface flow to the gauge (grey) as a function of UAA, with a visible threshold near about 10 ha. For both panels, lines show best-fit power law regressions to aid in interpretation of model results.

5.2 A Critical Comparison of Transferability and Limitations of River Corridor Modeling Approaches

To date, assessment and prediction of hydrologic connectivity in the river corridor can be grouped into three main approaches (Table 2): empirical upscaling, distributed modeling, and reduced-complexity modeling. First, empirical studies use on-the-ground observation or instrumentation to directly measure hydrologic

connectivity at scales ranging from reaches (Covino et al., 2011; Mallard et al., 2014; Zimmer and McGlynn, 2017) to entire networks (Godsey and Kirchner, 2014; Jensen et al., 2017). Measurements are regressed against hydrologic or geologic parameters (e.g., stream discharge, upslope accumulated area) and used to estimate processes along the entire river corridor. Relatively few empirical studies have been published because they are field intensive, requiring substantial commitments of people's time to conduct field campaigns. Additionally, empirical relationships are not readily transferable to other locations with different geologic settings, catchment topologies, and hydrologic forcing. Still, these empirical studies directly observe the processes of interest. Recent work by Arismendi et al. (2017) demonstrates the potential for advanced statistical techniques (e.g., Hidden Markov Models) as another strategy for upscaling empirical findings. Other researchers have used a similar upscaling approach but replaced direct empirical observations with simulation results from mechanistic models. In these efforts, data from numerical studies are regressed against geologic or hydrologic characteristics, with regressions used to describe hydrologic processes as a function of readily observable properties of the landscape (e.g., Kiel and Cardenas, 2014). The major strength of these approaches is their rapid scaling to the stream network and ability to consider a variety of independent variables which thereby enables upscaling of small-scale processes to entire stream networks (Gomez-Velez et al., 2015; Gomez-Velez and Harvey, 2014; Kiel and Cardenas, 2014). These efforts assume that the processes of interest can be reasonably predicted from some measure of landscape form, but do not account for feedbacks that may occur among smaller-scale processes nor limitations due to the larger-scale context of the process (Stonedahl et al., 2013, 2010; Schmadel et al., 2017). To date, these studies lack any dynamic processes.

Fully distributed "top-down" hydrologic models can represent dynamic, spatially explicit exchanges in the river corridor (Frei et al., 2009; Wondzell et al., 2009a; Yu et al., 2016). Models in this class can represent processes across a suite of interacting spatial and temporal scales. However, these models are limited by the number of parameters required to inform the processes being simulated. As a result, non-unique parameters prevent the identification of a single best solution (e.g., Beven, 1993, 2006; Beven and Binley, 1992). Such models suffer from over-parameterization and a lack of the necessary data to parameterize the natural world at all relevant scales for all of the processes that are represented.

The reduced-complexity model derived and applied in this study is concerned with mechanistic representation of the hydrologic processes perceived to be dominant in the river corridor. As such, the model only includes the most dominant processes identified in the perceptual model. Obviously, many processes cannot be included – ones that are not considered dominant at our scale of interest or for the purposes for which the model was conceived and constructed. One clear example in this study is the parameterization of channel-unit scale exchange. In our model we simplify exchange at scales smaller than the 5-m valley discretization into the sum of the net up- or downwelling exchange flux and the $Q_{subgrid}$ terms. Although channel-unit scale exchange has been extensively studied (see review by Boano et al., 2014), it is not a dominant mechanism for prediction of network expansion and

contraction at the scales considered here. Still, future improvements could add sub-discretization exchange parameterized by metrics derived from topography (e.g., streambed concavity; Anderson et al., 2005) or based on empirical relationships derived for bedforms and individual features (e.g., Gomez-Velez et al., 2015). These processes would need to be included if the model were applied to predict reactive transport, particularly where exchanges with short timescales are the most important for reactive processes. Likewise, improved representation of heterogeneity in the valley colluvium thickness (T) and hydraulic conductivity (K) would likely improve the ability of the model to reflect site-specific patterns in intermittency (Fleckenstein et al., 2007).

The model also greatly simplifies hillslope-valley floor-stream connectivity. We assumed that lateral inflows would proportional to UAA, and implicitly assume that these inflows will be instantaneously synchronized with Q_{gauge}. Several existing studies consider spatial and temporal variability in hillslope discharge to valley bottoms (e.g., Jencso et al., 2009; Smith et al., 2013) and could potentially be integrated to improve the representation of those inputs. We elected not to parameterize these processes, nor the many others that are omitted or simplified, because they would increase data needs and are not considered dominant processes in our perceptual model of network expansion and contraction. Of course, processes not included in the perceptual model may be incorrectly omitted. In this case, iterative advances of hypotheses, field observations, and mechanistic models are important to correct these deficiencies.

1063 **Table 2: Summary of three approaches to simulate river corridor exchange at**
1064 **the scale of networks**

Approach	**Empirical Upscaling**	**Reduced-complexity modeling**	**Distributed Modeling**
Hydrologic Philosophy	Observational, empiricism	Bottom-up, Dominant process	Top-down
Complexity and data needs	Low	Moderate	Extensive
Description	(1) conduct field or numerical experiments; (2) regress metrics describing process (e.g., fluxes) against measureable explanatory variable(s); (3) assign the resultant property of interest to river corridor; (4) aggregate along river corridor.	Representation of the most important processes at scales relevant to the hydrologic question of interest.	Fully-coupled representation of process dynamics spanning multiple spatial and temporal scales. Mechanistic predictions of hydrologic dynamics in the river corridor as a function of the full suite of geologic setting and hydrologic forcing.
Geologic Setting	Independent variable(s) for regression	Parameterization of physical properties	Parameterization of physical properties
Hydrologic Forcing	Q may be used as an explanatory variable	Time-variable lateral inflows are a function of Q_{gauge}	Explicitly represented, based on observed meteorology
Physically-based	No	Yes	Yes
Strengths	Based on site-specific observations	Dynamic hydrology	Representation of interacting, multi-scale hydrologic processes; dynamic hydrology
Limitations	Steady-state hydrology	Omits processes perceived to be unimportant, which may reflect incorrect assumptions	Extensive parameterization
Examples in the river corridor	Covino et al., 2011; Gomez-Velez et al., 2015; Gomez-Velez and Harvey, 2014; Kiel and Cardenas,	Bencala and Walters, 1983; This study	Frei et al., 2009; Wondzell et al., 2009a; Yu et al., 2016

	2014; Mallard et al., 2014; Stewart et al., 2011; Zimmer and McGlynn, 2017; Jensen et al., 2017; Arismedni et al., 2017		

5.3 Potential Applications for Assessment of Connectivity in the River Corridor

"*Although the fine scales of field and laboratory studies are best suited to identifying the fundamental physical and biological processes, that understanding must be successfully linked to cumulative effects at watershed to regional and continental scales."* Harvey and Gooseff (2015)

Improved understanding of dynamic hydrologic connectivity along the river corridor is increasingly of interest to water resource researchers and managers in the U.S (e.g., Department of Defense, Environmental Protection Agency, 2014). In the wake of the Rapanos v. U.S. (2006) decision, new tools are needed to quantify connectivity along river networks and thus provide both a scientific and legal basis for river corridor management. For example, Caruso (2015) proposes the development of connectivity indices based on statistical descriptors of discharge, topology, and topography, but lacks any mechanistic predictive power and requires extensive data collection at each point to be evaluated. In contrast, this study represents an advance in the application of hydrologic science to inform river corridor management. The relatively low data needs enable this framework to be transferable and readily implemented to assess connectivity along the river corridor. As with any model, an initial implementation based on uncalibrated parameter estimates would provide only a preliminary assessment of connectivity. Site-specific parameterization, calibration, and validation would be required to use this model as the sole basis for management efforts.

In the Pacific Northwestern United States, the management of the river corridor increasingly depends upon understanding channel network expansion and contraction. One critical location in the river corridor is the "perennial initiation point" or "perennial flow initiation point", defined as the farthest upslope location with flow during summer low-flow conditions (Jaeger et al, 2007). Current practices attempt to construct empirical models to predict the locations of the perennial initiation points as a function of drainage area, lithology, land use, and other readily identifiable independent variables (e.g., Jaeger et al., 2007; Clark et al., 2008; Wood et al., 2009). Comparisons among empirical predictions, reduced-complexity model predictions, and distributed model predictions of intermittency will help develop an improved basis for management in unobserved locations.

We envision two immediate applications of the reduced complexity model presented here. First, the model could be used to design field studies. Initial model analyses could use feasible ranges of parameters (e.g., hydraulic conductivity, sediment thickness) to determine key locations that appear to control the potential expansion, contraction, and changes in connectivity along the river corridor. Similarly, sensitivity analyses could be used to identify the parameters with the greatest influence on model projections. These results could then be used to plan

field campaigns that would improve estimates of key parameters or identify the places and times when observations of intermittency or network extent may be most important. This approach could help make the most efficient use of limited resources that might be available for field work. Second, the model could be used as the basis of heuristic studies scaling up processes from reaches to entire networks. Indeed, the strategy of scaling reduced-complexity models to large networks—even in cases when acceptable validation data are not readily available—is emerging as an important area of research in the river corridor (e.g., Gomez-Velez et al., 2015). Current models do not include parametrization for mountain streams; this framework could form the basis of an upscaling strategy for high-gradient river networks.

6. Conclusions

The overall objective of this study was to predict dynamic hydrologic connectivity along the river corridor. To achieve this objective, we selected a well-studied headwater catchment to develop a perceptual model of river corridor exchange. Building on this perceptual model we next developed a reduced-complexity, mechanistic model to predict the dynamic hydrologic connectivity along the river corridor. The model developed may be of broad interest for hydrologists and water resource managers working in mountain river networks. While this study was designed to calibrate the reduced-complexity model by leveraging detailed, site-specific observations, we emphasize that the model was developed with potential transferability in mind. The reduced-complexity model has modest data requirements (stream discharge, catchment topography, reasonable estimates of hydrogeologic parameters) to generate an initial prediction at the river network scale. Calibration using site-specific observations of discharge, intermittency, and/or solute tracer studies can be implemented to refine predictions at sites of interest, as we demonstrate here. The framework is mechanistic, based on a state-of-the-science understanding of the river corridor in a mechanistic way, and is capable of simulating both hydrodynamics and solute transport. Additionally, the model is dynamic, enabling the simulation of network expansion and contraction. We expect the perceptual model detailed in this study is transferable to other mountain stream networks, where streams reflect down-valley discharge in excess of the down-valley capacity. Importantly, the reach-scale success of this approach also highlights the role that heterogeneity along a valley controls along-network connectivity. Variation in bedrock topography, hydraulic conductivity, and individual morphologic features result in a more complex pattern of connectivity that was captured by this model (Figs. S1, S2, S3). This result highlights the need for future study of these processes as controls on intermittency of stream flows.

In this study, we asked how geologic setting interacts with hydrologic forcing to produce spatial and temporal patterns of connectivity along the river corridor? We expected geologic controls to dominate periods of steady flow and hydrologic controls to be important only during highly dynamic periods (e.g., storm event responses). Instead, we found that geologic setting controls network dynamics during relatively low discharge conditions, and that the spatial patterns of lateral inflows arising from storage and release of water from hillslopes are dominant

during relatively wet periods. In contrast, connectivity in the river corridor is highly sensitive to hydrologic dynamics under the lowest flow conditions.

Acknowledgements

Data and facilities were provided by the H.J. Andrews Experimental Forest research program, funded by the National Science Foundation's (NSF's) Long-Term Ecological Research Program (DEB 1440409), US Forest Service Pacific Northwest Research Station, and Oregon State University. Wondzell was supported by NSF Grant No. EAR 1417603. Ward was supported by NSF Grant No. EAR 1652293. Tools for solute tracer time series analyses and spatial data processing were developed by Ward and others with support provided in part by NSF Grant Nos. EAR 1505309 and EAR 1331906. Ward was also supported by the Indiana University Office of the Vice Provost for Research and the Indiana Water Resources Research Center. This research was also supported in part by Lilly Endowment, Inc., through its support for the Indiana University (IU) Pervasive Technology Institute, and in part by the Indiana METACyt Initiative. The Indiana METACyt Initiative at IU is also supported in part by Lilly Endowment, Inc.

Any opinions, findings, and conclusions or recommendations expressed in this material are those of the authors and do not necessarily reflect the views of the National Science Foundation, U.S. Forest Service, or Indiana University.

Precipitation, discharge, and topographic data are available from the H.J. Andrews Experimental Forest Data Catalog (http://andrewsforest.oregonstate.edu/). Topographic survey and in-stream specific conductance data are available upon request to the corresponding author. The authors declare no conflicts of interest.

References

Amatya, D., Campbell, J., Wohlgemuth, P., Elder, K., Sebestyen, S., Johnson, S.L., Keppeler, E., Adams, M., Caldwell, P., Misra, D., 2016. Hydrological Processes of Reference Watersheds in Experimental Forests , USA, in: Amatya, D., Williams, T., Bren, L., de Jong, C. (Eds.), Forest Hydrology: Processes, Management and Assessment. CAB International, Oxfordshire, UK, pp. 219–239.

Arismendi, I., Dunham, J., Heck, M., Schultz, L., Hockman-Wert, D., 2017. A Statistical Method to Predict Flow Permanence in Dryland Streams from Time Series of Stream Temperature. Water 9, 946. doi:10.3390/w9120946

Bencala, K.E., Gooseff, M.N., Kimball, B.A., 2011. Rethinking Hyporheic Flow and Transient Storage to Advance Understanding of Stream-Catchment Connections. Water Resour. Res. 47, W00H03.

Bencala, K.E., Walters, R.A., 1983. Simulation of solute transport in a mountain pool-and-riffle stream: a transient storage model. Water Resour. Res. 19, 718–724. doi:10.1029/WR019i003p00718

Beven, K.J., 2006. A manifesto for the equifinality thesis. J. Hydrol. 320, 18–36.

Beven, K.J., 1993. Prophecy, reality and uncertainty in distributed hydrological modelling. Adv. Water Resour. 16, 41–51. doi:10.1016/0309-1708(93)90028-E

Beven, K.J., Binley, A.M., 1992. The future of distributed models: model calibration and uncertainty prediction. Hydrol. Process. 6, 279–298. doi:10.1002/hyp.3360060305

Boano, F., Harvey, J.W., Marion, A., Packman, A.I., Revelli, R., Ridolfi, L., Wörman, A., 2014. Hyporheic flow and transport processes: Mechanisms, models, and biogeochemical implications. Rev. Geophys. 52, 2012RG000417. doi:10.1002/2012RG000417.

Boulton, A.J., Findlay, S., Marmonier, P., Stanley, E.H., Valett, H.M., 1998. The functional significance of the hyporheic zone in streams and rivers. Annu. Rev. Ecol. Syst. 29, 59–81.

Bredehoeft, J.D., Konikow, L.F. 1993. Ground water models: validate or invalidate. Ground Water 31 (2), 178–179.

Brunke, M., Gonser, T., 1997. The ecological significance of exchange processes between rivers and groundwater. Freshw. Biol. 37, 1–33.

Burt, T.P., McDonnell, J.J., 2015. Whither field hydrology? The need for discovery science and outrageous hydrological hypotheses. Water Resour. Res. 51. doi:10.1016/0022-1694(68)90080-2

Cardenas, M.B., Zlotnik, V.A., 2003. Three-dimensional model of modern channel bend deposits. Water Resour. Res. 39, 1141.

Caruso, B.S., 2015. A hydrologic connectivity index for jurisdictional analysis of headwater streams in a montane watershed. Environ. Monit. Assess. 187. doi:10.1007/s10661-015-4862-2

Castro, J., Jackson, P., 2001. Bankfull discharge recurrence intervals and regional hydrualic geometry relationships.. J. Am. Water Resour. Assoc. 37, 1249–1262.

Castro, N.M., Hornberger, G.M., 1991. Surface-subsurface water interactions in an alluviated mountain stream channel. Water Resour. Res. 27, 1613–1621.

Clarke, S.E., Burnett, K.M., Miller, D.J., 2008. Modeling streams and hydrogeomorphic attributes in Oregon from digital and field data. J. Am. Water Resour. Assoc. 44,

459–477. doi:10.1111/j.1752-1688.2008.00175.x
Corson-Rikert, H.A., Wondzell, S.M., Haggerty, R., Santelmann, M. V, 2016. Carbon dynamics in the hyporheic zone of a headwater mountain streamin the Cascade Mountains, Oregon. Water Resour. Res. 52, 7556–7576. doi:10.1029/2008WR006912.M
Costigan, K. H., Jaeger, K. L., Goss, C. W., Fritz, K. M., and Goebel, P. C., 2016. Understanding controls on flow permanence in intermittent rivers to aid ecological research: integrating meteorology, geology and land cover. Ecohydrol., 9: 1141–1153. doi: 10.1002/eco.1712.
Covino, T.P., McGlynn, B.L., Mallard, J., 2011. Stream-groundwater exchange and hydrologic turnover at the network scale. Water Resour. Res. 47, W12521.
D'Angelo, D.J., Webster, J.R., Gregory, S. V, Meyer, J.L., Angelo, A.D.J.D., Webster, J.R., Gregory, S. V, Meyer, J.L., 1993. Transient Storage in Appalachian and Cascade Mountain Streams as Related to Hydraulic Characteristics. J. North Am. Benthol. Soc. 12, 223–235. doi:10.2307/1467457
Department of Defense, Environmental Protection Agency, 2014. Definition of "Waters of the United States" Under the Clean Water Act. Fed. Regist. 79, 22188–22247.
Dyrness, C.T., 1969. Hydrologic properties of soils on three small watersheds in the western Cascades of Oregon. USDA For. Serv. Res. Note PNW-111, SEP 1969. 17 P.
Elliott, A.H., Brooks, N.H., 1997a. Transfer of nonsorbing solutes to a streambed with bed forms: Laboratory experiments. Water Resour. Res. 33, 137–151.
Elliott, H., Brooks, N.H., 1997b. Transfer of nonsorbing solutes to a streambed with bed forms : Theory. Water Resour. Res. 33, 123–136.
Fernald, A.G., Wigington, P.J., Landers, D., 2001. Transient storage and hyporheic flow along the Willamette River, Oregon: Field measurements and model estimates. Water Resour. Res. 37, 1681–1694.
Fleckenstein, J.H., Niswonger, R.G., Fogg, G.E., 2006. River-aquifer interactions, geologic heterogeneity, and low-flow management. Ground Water 44: 837-852.
Frei, S., Fleckenstein, J.H., Kollet, S.J., Maxwell, R.M., 2009. Patterns and dynamics of river-aquifer exchange with variably-saturated flow using a fully-coupled model. J. Hydrol. 375, 383–393. doi:10.1016/j.jhydrol.2009.06.038
Godsey, S.E., Kirchner, J.W., 2014. Dynamic, discontinuous stream networks: Hydrologically driven variations in active drainage density, flowing channels and stream order. Hydrol. Process. 28, 5791–5803. doi:10.1002/hyp.10310
Gomez-Velez, J.D., Harvey, J.W., 2014. A hydrogeomorphic river network model predicts where and why hyporheic exchange is important in large basins 1–10. doi:10.1002/2014GL061099
Gomez-Velez, J.D., Harvey, J.W., Cardenas, M.B., Kiel, B., 2015. Denitrification in the Mississippi River network controlled by flow through river bedforms. Nat. Geosci. 8, 1–8. doi:10.1038/ngeo2567
Gooseff, M.N., Anderson, J.K., Wondzell, S.M., LaNier, J., Haggerty, R., 2006. A modelling study of hyporheic exchange pattern and the sequence, size, and spacing of stream bedforms in mountain stream networks, Oregon, USA. Hydrol. Process. 20, 2443–2457.

1271 Grayson, R., Bloschl, G. (eds), 2000. Spatial Patterns in Catchment Hydrology:
1272 Observations and Modeling. Cambridge University Press, Cambridge, UK.
1273 Gregory, K.J., Walling, D.E., 1968. the Variation of Drainage Density Within a
1274 Catchment. Int. Assoc. Sci. Hydrol. Bull. 13, 61–68.
1275 doi:10.1080/02626666809493583
1276 Harvey, J.W., Bencala, K.E., 1993. The effect of streambed topography on surface-
1277 subsurface water exchange in mountain catchments. Water Resour. Res. 29, 89–
1278 98.
1279 Harvey, J.W., Gooseff, M.N., 2015. River corridor science: Hydrologic exchange and
1280 ecological consequences from bedforms to basins. Water Resour. Res. Special
1281 Issue, 1–30. doi:10.1002/2015WR017617
1282 Henshaw, D., Creel, C. 2005. Andrews Experimental Forest Small Wa tershed Flume
1283 History. Available online at:
1284 https://andrewsforest.oregonstate.edu/sites/default/files/lter/data/studies/h
1285 f04/weir_descriptions.pdf. Accessed on 22-June-2017.
1286 Jackman, A.P., Walters, R.A., Kennedy, V.C., 1984. Transport and concentration
1287 controls for chloride, strontium, potassium and lead in Uvas Creek, a small
1288 cobble-bed stream in Santa Clara County, California, U.S.A.: 2. Mathematical
1289 modeling. J. Hydrol. 75, 111–141.
1290 Jaeger, K.L., Montgomery, D.R., Bolton, S.M., 2007. Channel and perennial flow
1291 initiation in headwater streams: Management implications of variability in
1292 source-area size. Environ. Manage. 40, 775–786. doi:10.1007/s00267-005-
1293 0311-2
1294 Jencso, K.G., McGlynn, B.L., Gooseff, M.N., Wondzell, S.M., Bencala, K.E., Marshall, L.A.,
1295 2009. Hydrologic connectivity between landscapes and streams: Transferring
1296 reach-and plot-scale understanding to the catchment scale. Water Resour. Res.
1297 45.
1298 Jensen, C.K., McGuire, K.J., Prince, P.S., 2017. Headwater stream length dynamics
1299 across four physiographic provinces of the Appalachian Highlands. Hydrol.
1300 Process. 31, 3350–3363. doi:10.1002/hyp.11259
1301 Kasahara, T., Wondzell, S.M., 2003. Geomorphic controls on hyporheic exchange
1302 flow in mountain streams. Water Resour. Res. 39, 1005.
1303 Kaser, D.H., Binley, A.M., Heathwaite, A.L., Krause, S., 2009. Spatio-temporal
1304 variations of hyporheic flow in a riffle-step-pool sequence. Hydrol. Process. 23.
1305 Kennedy, V.C., Jackman, A.P., Zand, S.M., Zellweger, G.W., Avanzino, R.J., Walters, R.A.,
1306 1984. Transport and concentration controls for chloride, strontium, potassium
1307 and lead in Uvas Creek, a small cobble-bed stream in Santa Clara County,
1308 California, USA: 2. Mathematical modeling. J. Hydrol. 75, 67–110.
1309 Kiel, B., Cardenas, M., 2014. Lateral hyporheic exchange throughout the Mississippi
1310 River network. Nat. Geosci. 7, 413–417. doi:10.1038/ngeo2157
1311 Krause, S., Hannah, D.M., Fleckenstein, J.H., Heppell, C.M., Kaeser, D., Pickup, R.,
1312 Pinay, G., Robertson, A.L., Wood, P.J., 2011. Inter-disciplinary perspectives on
1313 processes in the hyporheic zone. Ecohydrology 4, 481–499.
1314 Mallard, J., McGlynn, B., Covino, T., 2014. Lateral inflows, stream-groundwater
1315 exchange, and network geometry influence streamwater composition. Water
1316 Resour. Res. 50, 4603–4623. doi:10.1002/2013WR014222

1317 Malzone, J.M., Lowry, C.S., Ward, A.S., 2016. Response of the hyporheic zone to
1318 transient groundwater fluctuations on the annual and storm event time scales.
1319 Water Resour. Res. 52, 1–20. doi:10.1002/2014WR015716
1320 McGlynn, B.L., McDonnell, J.J., Brammer, D.D., 2002. A review of the evolving
1321 perceptual model of hillslope owpaths at the Maimai catchments , New
1322 Zealand 257.
1323 McGlynn, B.L., McDonnell, J.J., Shanley, J.., Kendall, C., 1999. Riparian zone flowpath
1324 dynamics during snowmelt in a small headwater catchment. J. Hydrol. 222, 75–
1325 92. doi:10.1016/S0022-1694(99)00102-X
1326 McGuire, K.J., McDonnell, J.J., Weiler, M., Kendall, C., McGlynn, B.L., Welker, J.M.,
1327 Seibert, J., 2005. The role of topography on catchment-scale water residence
1328 time. Water Resour. Res. 41, W05002.
1329 Merill, L., Tonjes, D.J., 2014. A Review of the Hyporheic Zone, Stream Restoration,
1330 and Means to Enhance Denitrification. Crit. Rev. Environ. Sci. Technol. 44,
1331 2337–2379. doi:10.1080/10643389.2013.829769
1332 Oreskes, N., Shrader-Frechette, K., Belitz, K., 1994. Verification, Validation, and
1333 Confirmation of Numerical Models in the Earth Sciences. Science. 263, 641-646.
1334 Packman, A.I., Bencala, K.E., 2000. Modeling surface-subsurface hydrological
1335 interactions, in: Jones, J.B., Mulholland, P.J. (Eds.), Streams and Ground Waters.
1336 pp. 45–80.
1337 Packman, A.I., Salehin, M., 2003. Relative roles of stream flow and sedimentary
1338 conditions in controlling hyporheic exchange. Hydrobiologia 494, 291–297.
1339 Packman, A.I., Brooks, N.H., 2001. Hyporheic exchange of solutes and colloids with
1340 moving bed forms. Water Resour. Res. 37, 2591–2605.
1341 Payn, R.A., Gooseff, M.N., McGlynn, B.L., Bencala, K.E., Wondzell, S.M., 2009. Channel
1342 water balance and exchange with subsurface flow along a mountain headwater
1343 stream in Montana, United States. Water Resour. Res. 45. W11427.
1344 Poeter, E., 2007. All Models are Wrong, How Do We Know Which are Useful? Ground
1345 Water 45, 390–391. doi:10.1111/j.1745-6584.2007.00350.x
1346 Rapanos v. United States. 547 US 715, (2006).
1347 Runkel, R.L. 1998. One-dimensional Transport with Inflow and Storage (OTIS): A
1348 Solute Transport Model for Streams and Rivers. US Dept. of the Interior, US
1349 Geological Survey; Information Services.
1350 Ryan, R.J., Packman, A.I., Welty, C., 2004. Estimation of solute transport and storage
1351 parameters in a stream with anthropogenically produced unsteady flow and
1352 industrial bromide input. Water Resour. Res. 40, W01602.
1353 Salehin, M., Packman, A.I., Paradis, M., 2004. Hyporheic exchange with
1354 heterogeneous streambeds: laboratory experiments and modeling. Water
1355 Resour. Res. 40, W11504.
1356 Sawyer, A.H., Cardenas, M.B., 2009. Hyporheic flow and residence time distributions
1357 in heterogeneous cross-bedded sediment. Water Resour. Res. 45, W08406.
1358 Schmadel, N. M., B. T. Neilson, J. E. Heavilin, D. K. Stevens, and A. Wörman, 2014.
1359 The influence of spatially variable stream hydraulics on reach scale transient
1360 storage modeling, Water Resour. Res., 50, 9287–9299,
1361 doi:10.1002/2014WR015440.
1362 Schmadel, N.M., Ward, A.S., Lowry, C.S., Malzone, J.M., 2016. Hyporheic exchange

controlled by dynamic hydrologic boundary conditions. Geophys. Res. Lett. 1–10. doi:10.1002/2016GL068286
Schmadel, N. M., A. S. Ward, S. M. Wondzell, 2017. Hydrologic controls on hyporheic exchange in a mountain stream, Water Resour. Res. 53, 6260-6278.
Schwanghart, W., Kuhn, N.J., 2010. TopoToolbox: A set of Matlab functions for topographic analysis. Environ. Model. Softw. 25, 770–781. doi:10.1016/j.envsoft.2009.12.002
Schwanghart, W., Scherler, D., 2014. Short Communication: TopoToolbox 2 - MATLAB-based software for topographic analysis and modeling in Earth surface sciences. Earth Surf. Dyn. 2, 1–7. doi:10.5194/esurf-2-1-2014
Sivapalan, M., 2003. Process complexity at hillslope scale, process simplicity at the watershed scale: is there a connection? Hydrol. Process. 17, 1037–1041. doi:10.1002/hyp.5109
Smith, T., Marshall, L., McGlynn, B., Jencso, K., 2013. Using field data to inform and evaluate a new model of catchment hydrologic connectivity. Water Resour. Res. 49, 6834–6846. doi:10.1002/wrcr.20546
Stanford, J.A., Ward, J. V., 1993. An ecosystem perspective of alluvial rivers: Connectivity and the hyporheic corridor. J. North Am. Benthol. Soc. 12, 48–60.
Stewart, R.J., Wollheim, W.M., Gooseff, M.N., Briggs, M. a., Jacobs, J.M., Peterson, B.J., Hopkinson, C.S., 2011. Separation of river network–scale nitrogen removal among the main channel and two transient storage compartments. Water Resour. Res. 47, W00J10.
Stonedahl, S.H., Harvey, J.W., Packman, A.I., 2013. Interactions between hyporheic flow produced by stream meanders, bars, and dunes. Water Resour. Res. 49, 5450–5461. doi:10.1002/wrcr.20400
Stonedahl, S.H., Harvey, J.W., Wörman, A., Salehin, M., Packman, A.I., 2010. A multiscale model for integrating hyporheic exchange from ripples to meanders. Water Resour. Res. 46, W12539. doi:10.1029/2009WR008865
Swanson, F.J., James, M.E., 1975. Geology and geomorphology of the H.J. Andrews Experimental Forest, Western Cascades, Oregon. Pacific Northwest Forest and Range Experiment Station, Forest Service, U.S. Dept. of Agriculture. Research Paper PNW-188.
Swanson, F.J., Jones, J.A., 2002. Geomorphology and hydrology of the HJ Andrews experimental forest, Blue River, Oregon. F. Guid. to Geol. Process. Cascadia 36, 289–314.
US EPA, 2015. Connectivity of Streams & Wetlands to Downstream Waters: A Review and Synthesis of the Scientific Evidence (Final Report). Washington, DC. doi:10.1017/CBO9781107415324.004
Vaux, W.G., 1968. Intragravel flow and interchange of water in a streambed. Fish. Bull. 66, 479.
Voltz, T.J., Gooseff, M.N., Ward, A.S., Singha, K., Fitzgerald, M., Wagener, T., 2013. Riparian hydraulic gradient and stream-groundwater exchange dynamics in steep headwater valleys. J. Geophys. Res. Earth Surf. 118, 953–969. doi:10.1002/jgrf.20074
Wagener, T., Sivapalan, M., Troch, P., Woods, R., 2007. Catchment Classification and Hydrologic Similarity. Geogr. Compass 1, 901–931. doi:10.1111/j.1749-

8198.2007.00039.x
Ward, A.S., Fitzgerald, M., Gooseff, M.N., Voltz, T.J., Binley, A.M., Singha, K., 2012. Hydrologic and geomorphic controls on hyporheic exchange during base flow recession in a headwater mountain stream. Water Resour. Res. 48, W04513.
Ward, A.S., Gooseff, M.N., Fitzgerald, M., Voltz, T.J., Singha, K., 2014. Spatially distributed characterization of hyporheic solute transport during baseflow recession in a headwater mountain stream using electrical geophysical imaging. J. Hydrol. 517, 362–377. doi:10.1016/j.jhydrol.2014.05.036
Ward, A.S., Gooseff, M.N., Johnson, P.A., 2011. How can subsurface modifications to hydraulic conductivity be designed as stream restoration structures? Analysis of Vaux's conceptual models to enhance hyporheic exchange. Water Resour. Res. 47, W08512. doi:10.1029/2010wr010028
Ward, A.S., Gooseff, M.N., Voltz, T.J., Fitzgerald, M., Singha, K., Zarnetske, J.P., 2013a. How does rapidly changing discharge during storm events affect transient storage and channel water balance in a headwater mountain stream? Water Resour. Res. 49, 5473–5486. doi:10.1002/wrcr.20434
Ward, A.S., Payn, R.A., Gooseff, M.N., McGlynn, B.L., Bencala, K.E., Kelleher, C. A., Wondzell, S.M., Wagener, T., 2013b. Variations in surface water - ground water interactions along a headwater mountain stream: Comparisons between transient storage and water balance analyses. Water Resour. Res. 3359-3374. doi:10.1002/wrcr.20148
Ward, A.S., Schmadel, N.M., Wondzell, S.M., Harman, C.J., Gooseff, M.N., Singha, K., 2016. Hydrogeomorphic controls on hyporheic and riparian transport in two headwater mountain streams during base flow recession. Water Resour. Res. 52, 1479–1497.
Ward, A.S., Kelleher, C.A., Mason, S.J.K., Wagener, T., McIntyre, N., McGlynn, B., Runkel, R.L., Payn, R.A. 2017. A software tool to assess uncertainty in transient-storage model parameters using Monte Carlo simulations. *Freshwater Sci.* 36, 195-217.
Whiting, J.A., Godsey, S.E., 2016. Discontinuous headwater stream networks with stable flowheads, Salmon River basin, Idaho. Hydrol. Process. 30, 2305–2316. doi:10.1002/hyp.10790
Wood, M.S., Rea, A., Skinner, K.D., Hortness, J.E., 2009. Estimating Locations of Perennial Streams in Idaho Using a Generalized Least-Squares Regression Model of 7-Day , 2-Year Low Flows: U.S. Geological Survey Scientific Investigations Report 2009–5015.
Wondzell, S.M., 2011. The role of the hyporheic zone across stream networks. Hydrol. Process. 25, 3525–3532. doi:10.1002/hyp.8119
Wondzell, S.M., 2006. Effect of morphology and discharge on hyporheic exchange flows in two small streams in the Cascade Mountains of Oregon, USA. Hydrol. Process. 20, 267–287.
Wondzell, S.M., Gooseff, M.N., 2014. Geomorphic Controls on Hyporheic Exchange Across Scales: Watersheds to Particles, in: Schroder, J., Wohl, E. (Eds.), Treatise on Geomorphology. Academic Press, San Diego, CA, pp. 203–218.
Wondzell, S.M., Gooseff, M.N., McGlynn, B.L., 2010. An analysis of alternative conceptual models relating hyporheic exchange flow to diel fluctuations in

discharge during baseflow recession. Hydrol. Process. 24, 686–694.
Wondzell, S.M., Gooseff, M.N., McGlynn, B.L., 2007. Flow velocity and the hydrologic behavior of streams during baseflow. Geophys. Res. Lett. 34, L24404. doi:10.1029/2007GL031256
Wondzell, S.M., LaNier, J., Haggerty, R., 2009a. Evaluation of alternative groundwater flow models for simulating hyporheic exchange in a small mountain stream. J. Hydrol. 364, 142–151.
Wondzell, S.M., LaNier, J., Haggerty, R., Woodsmith, R.D., Edwards, R.T., 2009b. Changes in hyporheic exchange flow following experimental wood removal in a small, low-gradient stream. Water Resour. Res. 45, W05406.
Wondzell, S.M., Swanson, F.J., 1996. Seasonal and storm dynamics of the hyporheic zone of a 4 th-order mountain stream. 2: Nitrogen cycling. J. North Am. Benthol. Soc. 15, 3–19.
Wörman, A., Packman, A.I., Jonsson, K., Wörman, A., Johansson, H., 2002. Effect of flow-induced exchange in hyporheic zones on longitudinal transport of solutes in streams and rivers. Water Resour. Res. 38, 1–15.
Wright, K.K., Baxter, Li, J.L., 2005. Restricted hyporheic exchange in an alluvial river system: implications for theory and management. J. North Am. Benthol. Soc. 24, 447–460.
Yu, X., Duffy, C., Gil, Y., Leonard, L., Bhatt, G., Thomas, E., 2016. Cyber-Innovated Watershed Research at the Shale Hills Critical Zone Observatory. IEEE Syst. J. 10, 1239–1250. doi:10.1109/JSYST.2015.2484219
Zimmer, M.A., McGlynn, B.L., 2017. Ephemeral and intermittent runoff generation processes in a low relief, highly weathered catchment. Water Resour. Res. 53, 7055–7077. doi:10.1002/2016WR019742